Electronic Structure Studies of Palladium Sulphide (PdS) and Platinum (Pt) Ternaries

A thesis presented

by

Nkwe Oscar Monama

to

The Department of Physics

In fulfillment of the requirements for the degree of

Master of Science in the subject of

Physics

Faculty of Science, Health, and Agriculture

School of Physical and Mineral Sciences

University of Limpopo (Turfloop campus)

South Africa

Supervisor: **Professor P.E. Ngoepe**

[May] [2008]

Abstract

We present first principles structural, electronic and optical properties investigation of PdS, which are carried out using density functional theory under plane wave pseudopotential method within the local density approximation. We used ultrasoft-pseudopotentials to carry out our calculations. Calculated lattice parameters of the system show excellent agreement with the experimental values. The lattice parameters were observed to decrease linearly with increasing pressure. The density of states and optical properties of PdS have been computed under hydrostatic pressure. The actual size of the band gap remains constant with increasing pressure, whilst the peaks just below and above the Fermi energy moves to the left and to the right respectively. We also investigated the effect of compositional variation on our reflectance by calculating the reflectivity of $Pd_{4-x}Pt_xS_4$ and $Pd_{4-x}Ni_xS_4$. Since we have different positions for the same concentration, we used the heats of formation to determine the most stable structures and these structures were used to study the effect of compositional variation on our reflectance spectrum. We studied the equation of state (EOS), structure under hydrostatic pressure, and deduced the bulk modulus. It is important to study these properties under such extreme conditions of pressure and temperature as they tend to occur below the earth's surface. Investigation of stability and mechanical properties of binary and ternary compounds from PtS to PdS have been carried out, were the presence of the miscibility

gap is still uncertain. We investigate stability of these compounds by studying the heats of formation, elasticity and electronic properties. Our results show no miscibility gap but continuum solid solution between these compounds. A shift of the Fermi energy towards the conduction band is observed at a 50% concentration of Pd and Pt. All the information obtained on PdS is intended to assist in fitting interatomic potentials to enable studies of systems with many atoms.

Declaration

I declare that the dissertation hereby submitted to University of Limpopo for the degree of Master of Science has not been previously submitted by me for a degree at this or any university, and that the work herein is originally my own. All material contained therein has been duly acknowledged.

_____

Nkwe Oscar Monama

Acknowledgments

I would like to take this opportunity to thank my supervisor: Professor Ngoepe P.E. for the initiation of the project, wonderful support, patience, encouragement and discussions. The calculations on this thesis were done at the Materials Modeling centre (MMC) in the University of Limpopo, Turfloop campus. I received a great support from the team work involved in the laboratory I was working in. I really appreciate the comfortable working environment and the cooperation as well as the fruitful discussions.

I thank the sponsors of this project: University of Limpopo (UL) and the National Research Foundation (NRF).

Thanks to my family for the patience they have shown, coupled with encouragement and support. Not forgetting all friends who gave me the wonderful support over the period of my study.

Dedication

This work is dedicated to:

My **W**ife
Lebogang

My **D**aughter
Mocheta

My **M**other
Mothibi

My **S**iblings
Mphephethi and **M**ashela

Ke a leboga Bakone!!

Contents

List of figures

List of tables

Chapter 1
Introduction

1.1 General introduction

Vysotskite (PdS) is one of the precious metal sulphides such as cooperite (PtS), braggite (Pt, Pd, Ni)S and sperrylite ($PtAs_2$). These minerals are an important source of platinum and palladium in the world's largest deposits of platinum-group minerals (PGM) [1] which also contain the sulfides of other transition metals such as Os, Ir, Ru, Pd, Fe, Ni and Cu [2]. The binary and higher sulphides of the platinum family metals have high potential for various technological applications (catalyst, acid-resistant high-temperature electrode, etc.) because of their special physicochemical properties. The enthalpy of formation of the binary palladium sulphides is important for the preparation and industrial application [3]. PdS shows new potential applications (lithographic films and plates, photographic films, catalytic photoelectrodes and solar cells) due to its electronic properties [4]. Folmer et al [5] reported some preliminary results about the photoelectrochemical properties of PdS single crystal. A Japanese patent has also reported PdS in a polymer matrix for solar cells [6]. Platinum group metals (particularly Pd and Pt) are used for low resistance ohmic contacts in semiconducting electron devices [7]. The mining industry is interested in electronic, magnetic, optical, structural and thermodynamic properties of platinum group

minerals since these affect ore formation, mineral processing and environmental mineralogy. However, as far as we know, little experimental work has been carried out on the behavior of PGM compounds. The formation of a deep pseudogap at the Fermi level is argued to be the driving electronic mechanism for the stabilization of Pt and Pd monosulphides. [8]. They play an important role as catalysts in the petroleum refining industry and recently, the plane-wave pseudopotential method has been used to study cohesion and electronic properties of a wide range of transition metal sulfides including the (Pt, Pd, Ni) sulphides. PGM represent the only known class of stable catalytic active phases for strongly sulpho-reduction hydroprocessing conditions. There is a correlation between the electronic structure and the catalytic activity for hydro-desulphurization: all TMS with a high HDS activity are semiconductors and tend to have a high degree of t_{2g} character in the highest occupied orbital [9]. These PGMs are an excellent hydrogenation and dehydrogenation catalyst. They can be alloyed and used in jewellery. The metal is used in dentistry, electrical contacts and in making surgical instruments.

1.2 Structural Aspects

The crystal structure of PdS is tetragonal with a space group P42/m, it has lattice parameters $a = 6.429$ Å, $c = 6.611$ and $\alpha = \beta = \gamma = 90°$ and a density of $\rho = 6.728$g/cm³. Atom Pd(1) sits in a slightly ruffled square of S atoms, while a rectangular plane coordinates atom Pd(2), and atom Pd(3) is both bent out of the plane and coordinate rectangular (see figure 1.1). Four Pd atoms in a distorted tetrahedron coordinate each S

atom [10]. It forms a complex tetragonal structure in which the Pd atoms form hexagon-triangle nets alternating with triangle-square nets occupied by the S atoms. The structure is usually thought to be controlled by high coordination [11]. Table 1.1 lists fractional coordinates, atom positions (Wyckoff notation) and equivalent isotropic thermal parameters of this mineral.

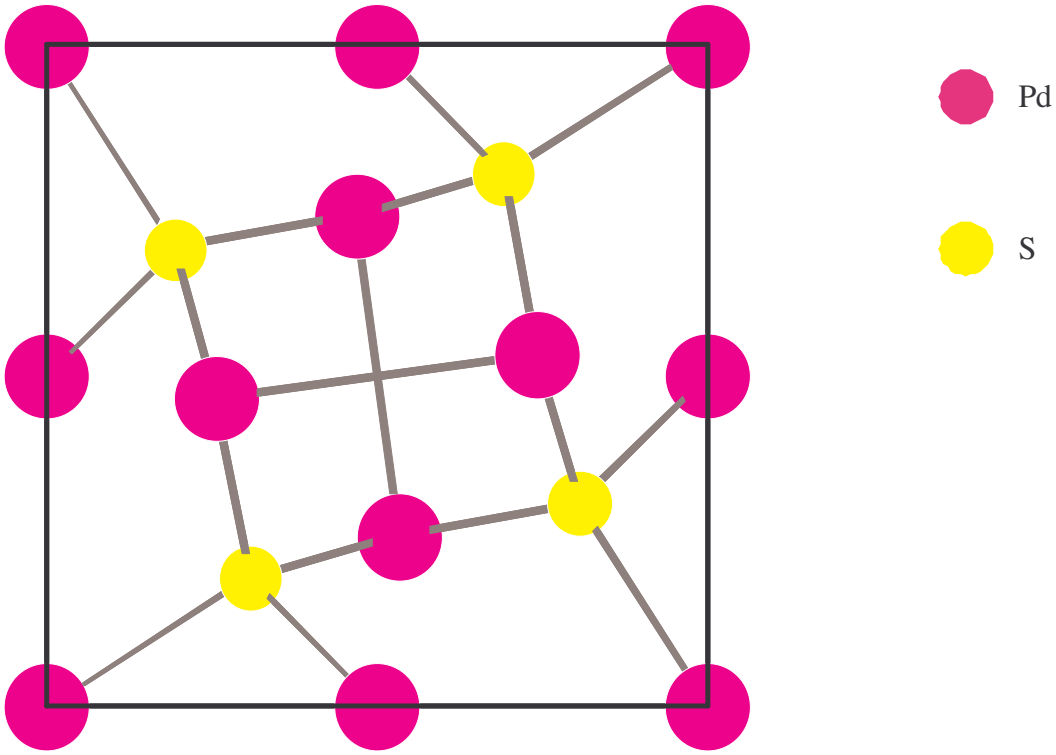

Figure 1.1 Crystal structure of PdS along [001] direction.

Table 1.1 Fractional coordinates atom position and equivalent isotropic thermal parameters for PdS

Atoms	Positions	x	y	z	B_{eq} (Å²)
Pd(1)	2a	(1/2)	0	0	0.35
Pd(2)	2e	0	0	(1/4)	0.33
Pd(3)	4j	0.257132	0.467792	0	0.33
S(1)	8k	0.307540	0.193610	0.22904	0.37

1.3 Literature Review

1.3.1 Structural Properties

In 1962, Genkin and Zvyagintsev [12] reported the mineral vysotskite, for which they indicated the formula (Pd,Ni)S, though they did not consider Ni to be an essential constituent. They found the mineral to be tetragonal with a = 6.371 Å and c = 6.540 Å, and the powder pattern was very similar to that reported for braggite. The powder pattern was also similar to that of synthetic PdS (Gaskell [13]) with lattice parameters a = 6.43 Å and c = 6.63 Å. A miscibility gap between cooperite and braggite [which is best described as (Pt,Pd ± Ni)S] was first documented by Cabri et al. [14]. A miscibility gap was proposed between braggite and vysotskite as well, which led to the redefinition of vysotskite as the Pt-Pd sulphides containing less that 10 mol% PtS [14]. This data suggested strongly that braggite and vysotskite were members of an isomorphous series, with PdS as an end-member. Figure 1.2 shows the PtS-PdS-NiS composition triangle.

Brese et al. [10] indicated that the square-planar coordination geometries about the Pd atoms are more regular than those reported in the classic structure of Gaskell [13]. The

geometry about atom Pd(2) is similar to that proposed by Childs and Hall [15] for the Pd site in braggite (Pt,Pd,Ni)S, although the Pd(2)-S distance at 2.318 Å is significantly longer than that of 2.26 Å in braggite.

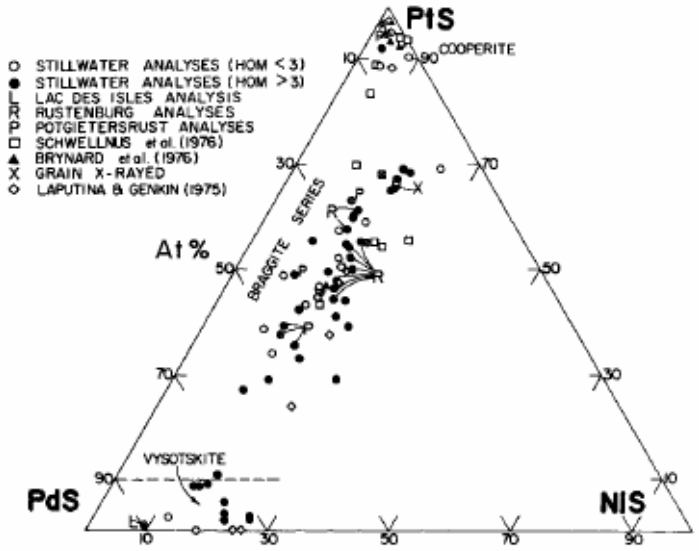

Figure 1.2 Cooperite, braggite, and vysotskite analyses plotted in the PtS-PdS-NiS composition triangle [14].

1.3.2 Electronic and Optical Properties

Electronic properties of a material help us to categorize the material within three main groups, namely, metals, semiconductors and insulator. The existence and the size of the gap between the highest occupied and the lowest unoccupied orbitals (energy gap) determine

the type of material. In case of a metal there is no band gap as there is an overlap of the orbitals, however for semiconductors and insulators a band gap exists which tends to be larger in insulators.

Semiconducting properties of PdS have been studied by various researchers and the band gap ranges between 0.05 eV and 2.0 eV [4, 7, 9]. Raybaud et al. [9] have shown that semiconducting transition metal sulphides, such as PdS, PtS, Rh_2S_3, Ir_2S_3 and RuS_2, have higher catalytic activity than the metallic sulphides. PdS and PtS have been employed as light receiving materials with silver halides [16, 17]. The reflectance of PdS is not lower than that of chalcopyrite as reported by Genkin [18], it is slightly higher, but nowhere near as high as reported by Vyalsov [19]. The dispersion of his reflectance spectrum for vysotskite is similar to that of Criddle and Stanley [1] but is inexplicably 7-8% higher. In plane-polarized light, in air and in oil, vysotskite has a slightly higher reflectance than braggite and is a slightly creamier white [1].

1.4 Intentions of the Study

The intention of the study is to use ab initio methods to study PdS. The density functional theory, within the local density approximation, will be used to callibrate the system by establishing kinetic energy cut-off, which will give accurate wave functions and hence electron charge distribution. The structural properties, which are lattice parameters, volume and bond lengths of the system will be determined. The electronic properties (density of state), optical properties (reflectivity and absorption), as well as the elastic properties

(elastic constant and bulk modulus etc.) will be calculated. The effect of pressure on electronic, optical and structural properties will be studied. Stability and mechanical properties of binary and ternary compounds from PtS to PdS will be investigated, where the presence of the miscibility gap is still uncertain. The stability of these compounds is investigated by studying the heats of formation, elasticity and electronic properties.

1.5 Outline of the Study

In this study, the density functional approach will be followed, using the ultrasoft-pseudopotential within the local density approximation (LDA).

Chapter 1, we introduce the topic and the content of this dissertation with the background of PdS and the motivation of the study.

Chapter 2, we explain the methods used in our study in details i.e. the classical, and quantum mechanics. These methods include plane-wave, pseudopotential approach.

Chapter 3, we discuss in details the results of our work on electronic, structural and optical properties. These results are compared to available experimental results.

Chapter 4, we discuss the issue of miscibility gap by looking at stability and mechanical properties of binary and ternary compounds from PtS to PdS.

Chapter 5, we make conclusion and recommendation. Finally, the bibliography which helps in giving the insight to the analysis of the work listed.

Chapter 2
Methodology

2.1 Introduction

Computational modeling offers another methodology of investigating properties of materials alongside experiments and theory. This approach is rapidly being broadly used in solid-state physics, chemistry, and material science. It presents physical systems as models, which are then simulated by computers to predict real situations. Availability of high performance computers has made modeling of systems with thousands of atoms possible. There are two types of computational approaches used for the prediction of material properties, namely, the quantum mechanical method (Density functional theory or Hartree-Fock theory) and empirical potential methods (atomistic method). The quantum mechanical methods take into account the motion and the interaction of electrons in a material whereas the empirical potential methods avoid the details of electronic structure and consider the interaction of atoms in a quasi-classical form.

In this work we have based our approach on quantum mechanical calculations, namely the density functional theory. Quantum mechanical methods are widely used as they can be used to study the structure, chemical, electrical, optical and magnetic properties of a material.

2.2 Ab Initio Methods

Ab initio, simply means first principle. Methods that require no empirical data but only specification of the ion present (by their atomic number) and the value of the fundamental physical constants such as mass and charge of electron, that is, it uses no experimental parameters in the computations. In these methods, molecules can be calculated using nothing but Schrödinger equation. Ab initio methods provide quality prediction for a wide range of systems, that is, metal, insulator, and semiconductors. The prediction of electronic and geometric structure requires the calculation of the quantum mechanical total energy of the system and minimization of that energy with respect to the electronic and nuclear coordinates. We require the solution of the time independent, non relativistic Schrödinger equation to calculate the total energy, electronic structure, and ground state properties of a system,

$$H\psi = E\psi \qquad (2.1)$$

Where H is the Hamiltonian and ψ is the wavefunction. However further simplification can be introduced to allow the energy to be calculated accurately. The methods include density functional theory, Hartree-Fork methods, etc, but we fully described density functional theory as it is the method we used in our study. The Hartree-Fork and Density Functional Theory are shown in figure 2.1

Hartree-Fock
(1928, 1930)

$$\psi(1,2,...N) \approx \psi_1(1)\cdot\psi_2(2)\cdot...\cdot\psi_N(N)+...$$

$$E = E[\psi]$$

$$E[\psi] = \frac{\int \psi^* H \psi \, d\tau}{\int \psi^* \psi \, d\tau}$$

$$\frac{\delta E}{\delta \psi_i} = 0$$

$$\Downarrow$$

$$[-\frac{1}{2}\nabla^2 + V_c + \mu_x^i]\psi_i = \varepsilon_i \psi_i$$

Hartree-Fork equations

Density Functional
(1964, 1965)

$$\psi^*\psi = \rho(r) = \sum_i \psi_i^* \psi_i$$

$$E = E[\rho]$$

$$E[\rho] = T_0[\rho] + U[\rho] + E_{xc}[\rho]$$

$$\frac{\delta E}{\delta \psi_i} = 0$$

$$\Downarrow$$

$$[-\frac{1}{2}\nabla^2 + V_c + \mu_{xc}]\psi_i = \varepsilon_i \psi_i$$

Kohn-Sham equations

Figure 2.1 The Hartree-Fork and Density Functional Theory (DFT) schemes [20, 21]. The DFT leads to the Kohn-Sham equation.

2.2.1 Density Functional Theory

Density functional theory (DFT) is based on concept by Thomas [22] and Fermi [23], they introduced an idea of expressing the total energy of a system as a functional of the total electron density. Due to the crude treatment of the kinetic energy term, that is, the absence of molecular orbitals, the accuracy of these early attempts was far from satisfactory. Density functional theory has been developed by Hohenberg and Kohn [24], and Kohn and Sham [25], who proved that the total energy including the exchange and correlation of an electron gas is a unique functional of the electron density. Earlier, motivated by the search for practical electronic structure calculations, Slater [26] had developed an approach, later to become the Xα method [27], which originally intended as an approximation to Hartree-Fock theory [28, 29]. Today, the Xα method is generally viewed as a simplified form or precursor of density functional theory.

For the past 30 years density functional theory has been the dominating method for the quantum mechanical simulation of periodic systems. Recently it has also been adopted by quantum chemist and it is widely used for the simulation of energy surfaces in molecules. This theory is used to study the structure, chemical, electrical, optical and magnetic properties of a material. An important advance in the calculation of the energy of electron of atoms and the force of each atom was made by Hohenberg and Kohn [24], who showed how a mean field theory could be applied to this problem. They proved that the total ground state energy of a many-electron body is a functional of the electron density $\rho(\vec{r})$, which in turn depends on the positions of atoms.

$$E = E[\rho(\vec{r}), \vec{R}_\alpha] \tag{2.2}$$

$\vec{R}_\alpha$ denotes the positions of all atoms α in the system under consideration. The Born-Oppenheimer approximation amounts to saying that we can separate the electronic and nuclear degree of freedom because the electronic mass is so much smaller than that of the nuclei the electrons respond almost instantaneously to the changes in the positions of the nuclei. It is then a good approximation to say the electrons are always in their ground state as the atoms of a solid vibrate thermally. This means that the positions of the nuclei are parameters that appear in the potential of the Schrödinger equation defining the wave functions of the electrons. This allowed Kohn and Sham [25] to derive an effective one-electron Schrödinger equation by comparing the functional as the sum of three terms written as

$$E[\rho] = T_0[\rho] + U[\rho] + E_{XC}[\rho] \tag{2.3}$$

where T_0 is the kinetic energy, U is the coulomb energy due to a classical electrostatic interactions among all charged particles in the system and E is the exchange correlation energy. The coulomb energy U which is purely classical contains the electrostatic energy arising from the coulombic attraction between electrons and nuclei, the repulsion between all electronic charges, and the repulsion between nuclei. It can be written as

$$U[\rho] = U_{en}[\rho] + U_{ee}[\rho] + U_{ion-ion} \tag{2.4}$$

The Hohenberg-Kohn-Sham theorem, states that the total energy is at its minimum value for the ground state density and that the total energy is stationary with respect to first-order

variations in the density, that is $\frac{\partial E[\rho]}{\partial \rho\big|_{\rho=\rho_0}} = 0$

In conjunction with the kinetic energy, one-particle wave function $\psi_i(\vec{r})$ is introduced that generate the electron density

$$\rho(\vec{r}) = \sum_i n_i \left|\psi_i\right|^2 \tag{2.5}$$

It is therefore necessary to determine the set of wave functions ψ_i that minimizes the Kohn-Sham energy function which is given by a self-consistent solution of the equation:

$$\left[-\frac{\hbar^2}{2m}\nabla^2 + V_{ion}(\vec{r}) + V_H(\vec{r}) + V_{XC}(\vec{r})\right]\psi_i(\vec{r}) = \varepsilon_i \psi_i(\vec{r}), \tag{2.6}$$

where ψ_i is the wave function of the electronic state i and ε_i is the Kohn-Sham eigenvalue, V_{ion} is the static total electron-ion potential and V_H is the Hartree potential of the electron which is given by

$$V_H = e^2 \int \frac{\rho(\vec{r}')}{\left|\vec{r} - \vec{r}'\right|} d^3\vec{r}' \tag{2.7}$$

and the exchange-correlation potential, V_{XC} is given by the functional derivative

$$V_{XC}(\vec{r}) = \frac{\delta E_{XC}[\rho(\vec{r})]}{\delta \rho(\vec{r})} \tag{2.8}$$

the electron density $\rho(\vec{r})$ is given by

$$\rho(\vec{r}) = 2\sum_i \int \left|\psi_i(\vec{r})\right|^2 \tag{2.9}$$

Hence, the Kohn-Sham total energy functional is written as

$$E = 2\sum_{occ} \varepsilon_i + U_{ion-ion} - \frac{e^2}{2}\iint \frac{\rho(\vec{r})\rho(\vec{r}')}{|\vec{r}-\vec{r}'|} d\vec{r}d\vec{r}' + E_{XC}[\rho(\vec{r})] - \int \rho(\vec{r}) V_{XC} d\vec{r} \qquad (2.10)$$

The exchange-correlation potential cannot be obtained explicitly because the exact exchange-correlation energy is unknown; therefore we need approximation methods to solve the problem. The commonly known approximation methods are LDA and GGA. We explain them in detail in sections 2.2.2 and 2.2.3 respectively. Figure 2.2 compares the methodology for solving the Schrödinger equation and the DFT Kohn-Sham equation respectively.

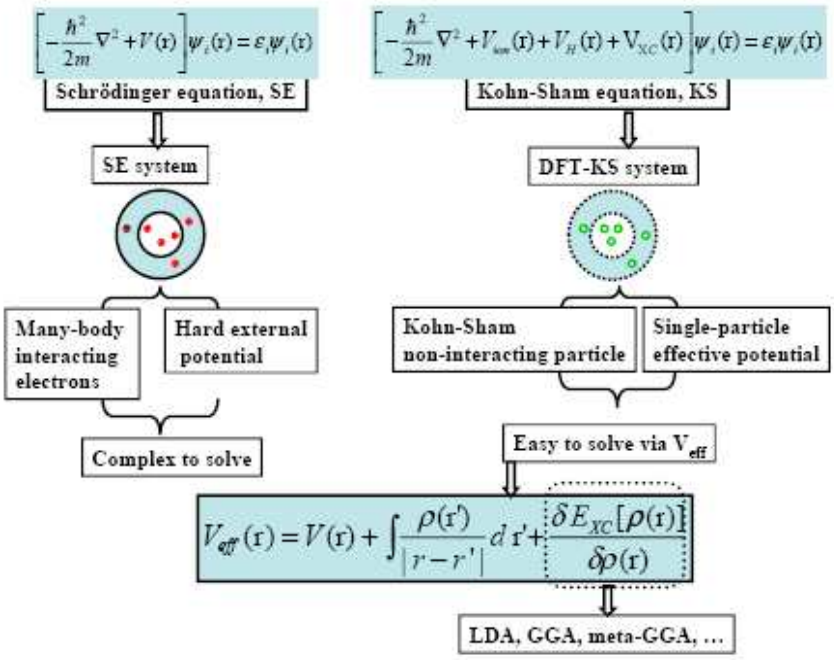

Figure 2.2 A comparison of the methodology for solving the many-body Schrödinger equation and effective one-electron Kohn-Sham equation [30]

2.2.2 Local Density Approximation

A common approximation is the so-called local density approximation (LDA) [24, 25], which locally substitutes the exchange-correlation energy density of an inhomogeneous system by that of an electron gas evaluated at the local density. The exchange-correlation energy depends only on the local electron density around each volume element $d\vec{r}$. The LDA rests on two basic assumptions: (i) the exchange and correlation effects come predominantly from the immediate vicinity of point $\vec{r}$ and (ii) these exchange and correlation effects do not depend strongly on the variations of the electron density in the vicinity of $\vec{r}$. If these two conditions are well fulfilled, then the contribution from volume element $d\vec{r}$ would be the same as if this volume element were surrounded by a constant electron density $\rho(\vec{r})$ of the same value as within $d\vec{r}$. Within LDA, the expression for the exchange-correlation energy can be written as

$$E_{XC}^{LDA}[\rho] = \int \rho(\vec{r})\varepsilon_{XC}[\rho(\vec{r})]d^3r \tag{2.11}$$

and

$$\frac{\delta E_{XC}^{LDA}(\rho(\vec{r}))}{\delta\rho(\vec{r})} = \frac{\partial[\rho(\vec{r})\varepsilon_{XC}(\vec{r})]}{\partial\rho(\vec{r})} \tag{2.12}$$

with

$$\varepsilon_{XC}(\vec{r}) = \varepsilon_{XC}[\rho(\vec{r})] \tag{2.13}$$

where $\varepsilon_{XC}[\rho(\vec{r})]$ is the exchange and correlation energy per electron of a uniform electron gas. Splitting this quantity into two parts we get:

$$\varepsilon_{XC}[\rho(\vec{r})] = \varepsilon_X[\rho(\vec{r})] + \varepsilon_C[\rho(\vec{r})] \tag{2.14}$$

The exchange part $\varepsilon_X[\rho(\vec{r})]$ can be derived analytically with the Hartree-Fork expression and be expressed as

$$\varepsilon_X[\rho(\vec{r})] = \frac{3}{4}\sqrt[3]{\frac{3\rho(\vec{r})}{\pi}} \tag{2.15}$$

The correlation part cannot be derived analytically, but can be calculated numerically with high accuracy by means of Monte Carlo simulations [31]. Figure 2.3 illustrates the basic idea. When performing the calculation LDA is known to underestimate the bond length in molecules and cell parameters in crystals [32]. The LDA uses the exchange-correlation energy for the uniform electron gas at every point in the system regardless of the inhomogeneity of the real charge density.

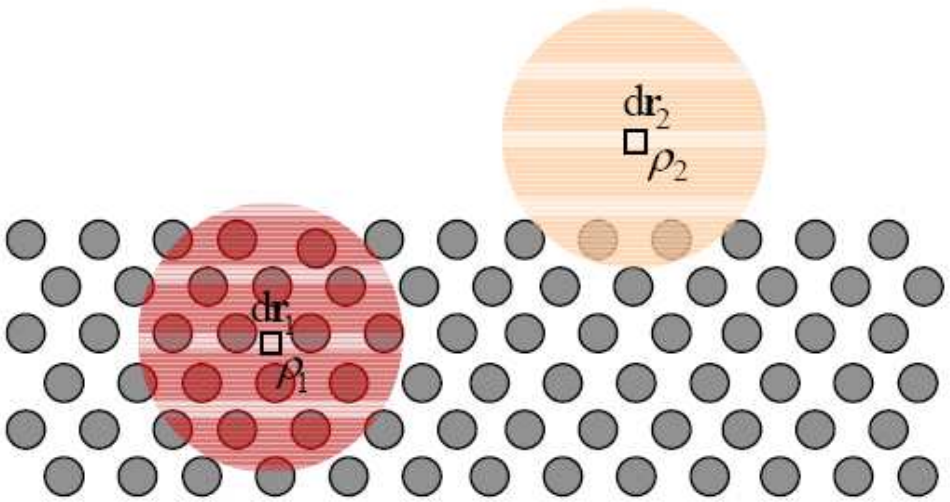

Figure 2.3 Illustration of the local density approximation (LDA). The solid dots represent positions of atomic nuclei; ρ_1 and ρ_2 denote the electron density in volume elements dr_1 and dr_2 respectively. In the LDA, it is assumed that for the evaluation of the exchange correlation effects, the real electron density surrounding each volume element can be replaced by a constant electron density of the same value as at the reference point. Note that this constant electron density is different for each point in space [20].

2.2.3 Generalized Gradient Approximation

For nonuniform charge densities the exchange-correlation energy can deviate significantly from the uniform result. This deviation can be expressed in terms of the gradient and higher spatial derivatives of the total charge density. The generalized gradient approximation (GGA) by Perdew [33], Becke [32], Perdew and Wang [34] and Perdew et al. [35] uses the gradient of the charge density, $\left|\nabla\rho(\vec{r})\right|$, to correct this deviation. The basic idea of GGAs is to express the exchange-correlation energy in the following form:

$$E_{XC}^{GGA}[\rho] = \int \rho(\vec{r})\varepsilon_{XC}[\rho(\vec{r})]dr + \int F_{XC}[\rho(\vec{r}), \nabla\rho(\vec{r})]d\vec{r} \tag{2.16}$$

where the function F_{XC} is asked to satisfy a number of formal conditions for the exchange correlation hole, such as sum rules, long-range decay and so on. The form suggested by Becke [32] for the exchange part is:

$$E_X^{GGA}[\rho_\uparrow, \rho_\downarrow] = E_X^{LDA} - \beta\sum_\sigma \int \frac{\rho_\sigma(\vec{r})^{\frac{4}{3}} x_\sigma^2}{1 + 6\beta x_\sigma \sinh^{-1} x_\sigma} d^3\vec{r} \tag{2.17}$$

where

$$E_X^{LDA} = -C_{X_\sigma} \sum \rho_\sigma^{\frac{4}{3}}(\vec{r}) d^3\vec{r}\,, \tag{2.18}$$

$C_X = \frac{3}{2}\left(\frac{3}{4\pi}\right)^{\frac{1}{3}}$, $X_\sigma = \left|\nabla\rho\right| \Big/ \rho_\sigma^{\frac{4}{3}}$, and σ denotes either $\uparrow$ or $\downarrow$ electron spin. The constant β is a parameter fitted to obtain the correct exchange energy of the noble gas atoms. For systems where the charge density is slowly varying, the GGA has proved to be an improvement over LDA. Gradient corrected density functionals have been studied

extensively for molecular systems, for example by Andzelm and Wimmer [36]. The following correlation functional as proposed by Perdew and Wang [34] predicts correlation energies of useful accuracy for an electron gas with slowly varying density:

$$E_X^{GGA}[\rho_\uparrow, \rho_\downarrow] = \int \rho(\vec{r}) \varepsilon_C(\rho_\uparrow, \rho_\downarrow) d^3\vec{r} + \int \frac{C_C(\rho)\left|\nabla\rho(\vec{r})\right|^2}{de^\phi \rho(\vec{r})^{\frac{4}{3}}} d^3\vec{r} \qquad (2.19)$$

where

$$d = 2^{\frac{1}{3}}\left[\left(\frac{1+\zeta}{2}\right)^{\frac{5}{3}} + \left(\frac{1-\zeta}{2}\right)^{\frac{5}{3}}\right], \qquad (2.20)$$

$$\phi = 0.1929\left[\frac{C_C(\infty)}{C_C(\rho)}\right]\frac{\left|\nabla\rho\right|}{\rho^{7/6}}, \qquad (2.21)$$

$\zeta = (\rho_\uparrow - \rho_\downarrow)/\rho$ and $C_C(\rho)$ is a rational polynomial of the density that contains seven fitting parameters. The correlation energy per particle of the uniform electron gas, $\varepsilon_C = (\rho_\uparrow, \rho_\downarrow)$, is taken from a parametrization by Perdew and Zunger [37] of the Cerperly-Alder [38] Monte Carlo results. Perdew-Burke-Ernzerhof writes the exchange functional in the form that contains an explicit enhancement factor F_{x} over the local exchange factor, this is normally known as GGA-PBE, is of the form:

$$E_X^{PBE}[\rho_\uparrow, \rho_\downarrow] = \int \rho(\vec{r}) \varepsilon_X^{LDA}[\rho(\vec{r})] F_{XC}(\rho, \xi, s) d\vec{r}\,, \qquad (2.22)$$

where ρ is the local density, ξ is the relative spin polarization, and $s = \left|\nabla\rho(\vec{r})\right|/(2k_F\rho)$ is the dimensionless density gradient. The enhancement factor is given by:

$$\left(sF_X = \left(\frac{1}{k + s^2\mu}\left(k + s^2\mu + s^2 k\mu\right)\right)\right) \tag{2.23}$$

where $\mu = \beta\left(\frac{\pi^2}{3}\right) = 0.21951$ with $\beta = 0.066725$. The correlation energy on the other hand is written in the form:

$$E_C^{PBE}[\rho_\uparrow, \rho_\downarrow] = \int \rho(\vec{r})\left[\varepsilon_C^{LDA}(\rho,\zeta) + H(\rho,\zeta,t)\right]d\vec{r} \tag{2.24}$$

with

$$H(\rho,\zeta,t) = \gamma\phi^3 In\left\{1 + \frac{\beta\gamma^2}{t}\left[\frac{1 + At^2}{1 + At^2 + A^2t^4}\right]\right\} \tag{2.25}$$

Here, $t = \left|\nabla\rho(\vec{r})\right|/(2k_s\rho)$ is the dimensionless density gradient, $ks = \left(\frac{4k_F}{\pi}\right)^{\frac{1}{2}}$ is the TF screening wave number and $\phi(\zeta) = \left[(1+\zeta)^{\frac{2}{3}} + (1-\zeta)^{\frac{2}{3}}\right]$ is a spin-scaling factor. The quantity β is the same for the exchange term $\beta = 0.066725$, and $\gamma = 0.031091$. The function A is of the form:

$$A = \frac{\beta}{\gamma}\left[e^{\varepsilon_C^{LDA}[\rho]/\gamma\phi^3} - 1\right]^{-1} \tag{2.26}$$

The iterative, self-consistent procedure for solving the Kohn-Sham equation is shown in figure 2.4 and the electronic structure methods are also summarized in figure 2.5.

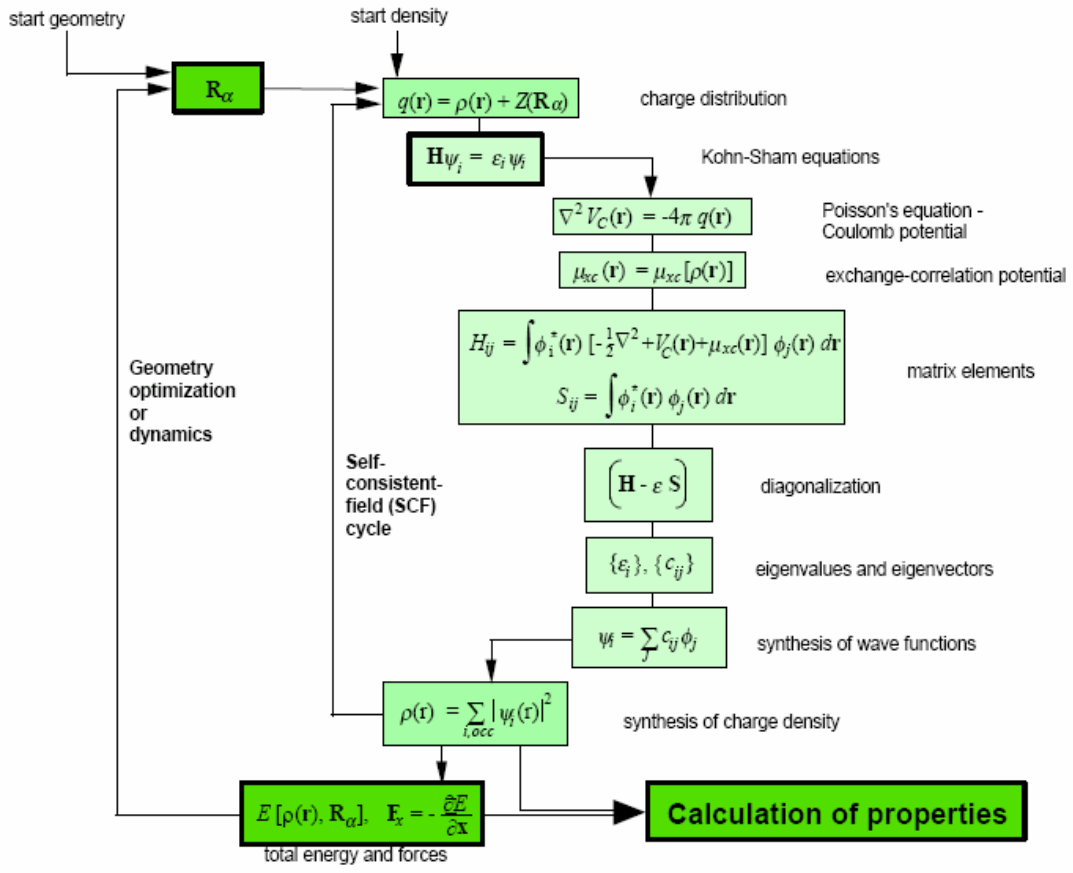

Figure 2.4 Scheme of typical electronic structure calculations. The outer cycle represents the geometry optimization or other manipulation of the geometry such as energy minimization, simulated annealing, dynamic trajectories or Monte Carlo procedures. The inner cycle is the self-consistent procedure to solve the Kohn-Sham equations [20]

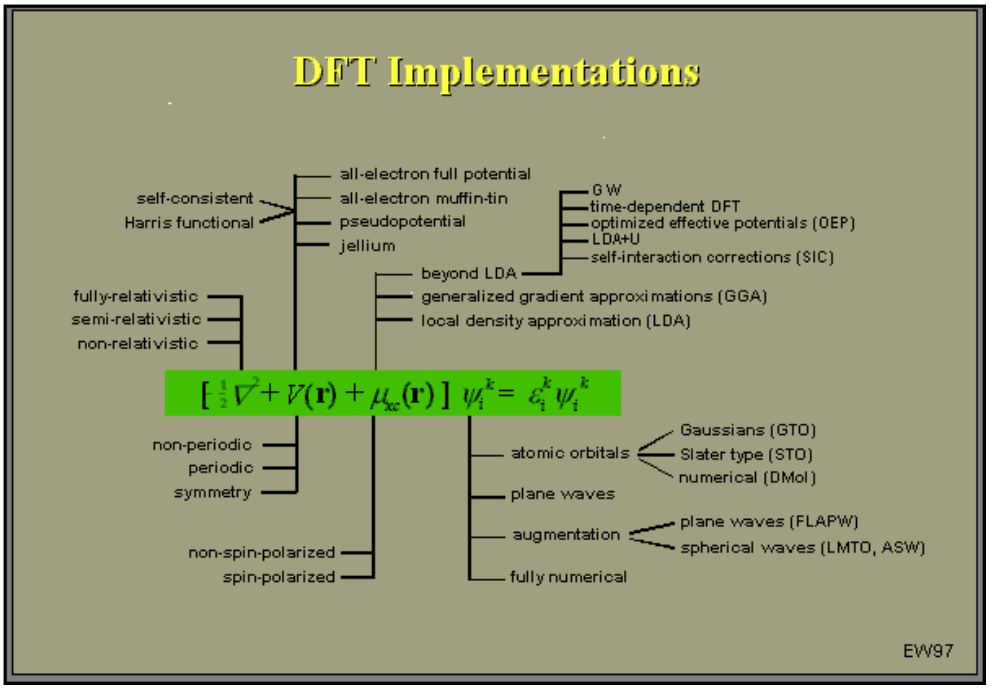

Figure 2.5 Overview of electronic structure methods for solving the Kohn-Sham equation [39]

2.3 Plane-Wave Pseudopotential Method

The plane-wave pseudopotential method is a technique that can be used to calculate with accuracy the variation self-consistent solution to the density functional theory. In this technique the wave function is expanded in terms of the plane-wave basis. The plane-wave pseudopotential method deals with weak pseudopotentials and performs full geometry optimization, particularly the internal parameters relaxation and it is capable of simulating electronic ground states for metals, insulators or semiconductors. Hence predicting with accuracy the forces acting on atoms and the stress on unit cells.

2.3.1 Plane-wave Basis

Since there are an infinite number of electrons, a wave function is needed for each. However, the basis set that is required to expand each wave function is infinite. These problems can be handled by performing calculations on periodic systems applying the Bloch's theorem which allows the electronic wave function to be expanded in terms of a discrete set of plane waves. The electronic wave functions of a periodic solid can be written as

$$\psi_i(\vec{r}) = \exp[i\vec{k}.\vec{r}]f_i(\vec{r}) \tag{2.27}$$

From this we can write the planewave whose wave vectors are reciprocal lattice vectors of the crystal as

$$f_i(\vec{r}) = \sum_{\vec{G}} C_{i,\vec{G}} \exp[i\vec{G}.\vec{r}] \tag{2.28}$$

where $\vec{G}$ is the reciprocal lattice vector of the periodic cell. $\vec{G}$ is required for the resolution of rapid variations in the wavefunctions and charge density. Hence each electronic wave function can be written as a sum of plane waves,

$$\psi_i(\vec{r}) = \sum_G C_{i,\vec{k}+\vec{G}} \exp[i(\vec{k}+\vec{G}).\vec{r}], \tag{2.29}$$

where $C_{i,\vec{k}+\vec{G}}$ are the coefficients for the plane waves. These coefficients depend on the specific kinetic energy, $\frac{\hbar^2}{2m}\left|\vec{k}+\vec{G}\right|^2$. The plane wave basis set is limited by including all plane waves whose kinetic energies are less than some particular energy cutoff, E_{cut}. Thus only the plane waves that obey

$$\frac{\hbar^2}{2m}\left|\vec{k}+\vec{G}\right|^2 < E_{cut} \tag{2.30}$$

are included in the basis. The plane wave set at a finite cutoff energy will lead to an error in the computed total energy; therefore the energy cutoff should be increased until the calculated energy has converged. It will be wise to use as much denser set of k-points to reduce errors and ensure convergence. Now substituting equation 2.29 into 2.6, the Kohn-Sham equation then takes the form

$$\sum\left[\frac{\hbar^2}{2m}\left|\vec{k}+\vec{G}\right|^2 \delta_{GG'} + V_{ion}(\vec{G}-\vec{G}') + V_H(\vec{G}-\vec{G}') + V_{XC}(\vec{G}-\vec{G}')\right] C_{i,\vec{k}+\vec{G}'} = \varepsilon_i C_{i,\vec{k}+\vec{G}} \tag{2.31}$$

The kinetic energy is diagonal, whereas the various potential contributions are given by their Fourier transforms. Solution of equation 2.31 proceeds by diagonalization of a Hamiltonian matrix whose matrix elements $H_{\vec{k}+\vec{G},\vec{k}+\vec{G}'}$ are given by the terms in brackets

above. The size of the matrix is determined by the choice of cutoff energy $\frac{\hbar 2}{2m}\left|\vec{k}+\vec{G}_c\right|^2$, and will be intractably large for the systems that contain both valence and core electrons.

2.3.2 Pseudopotentials

It has been shown by the use of Bloch's theorem, that a plane wave energy cut-off in the expansion of the wavefunction and careful k-points sampling that the solution to the Kohn-Sham equations for infinite crystalline systems is now tractable. Unfortunately a plane wave basis set is usually very poorly suited to expanding the electronic wavefunctions because a very large number are required to accurately describe the rapidly oscillating wavefunctions of electrons in the core region.

It is well known that most physical properties of solids are much dependable on the valence electrons than that of the tightly bound core electrons, that it why the pseudopotential approximation [41, 42, 43] is introduced. This approximation uses this fact to remove the core electrons and the strong nuclear potential and replace them with a weaker pseudopotential which acts on a set of pseudo wavefunctions rather than the true valence wavefunctions. In fact, the pseudopotential can be optimized so that, in practice, it is even weaker than the frozen core potential [44].

The schematic diagram in Figure 2.6 shows these quantities. The valence wavefunctions oscillate rapidly in the region occupied by the core electrons because of the strong ionic potential. These oscillations maintain the orthogonality between the core and valence electrons. The pseudopotential is constructed in such a way that there are no radial nodes in

the pseudo wavefunction in the core region and that the pseudo wavefunctions and pseudopotential are identical to the all electron wavefunction and potential outside a radius cut-off.

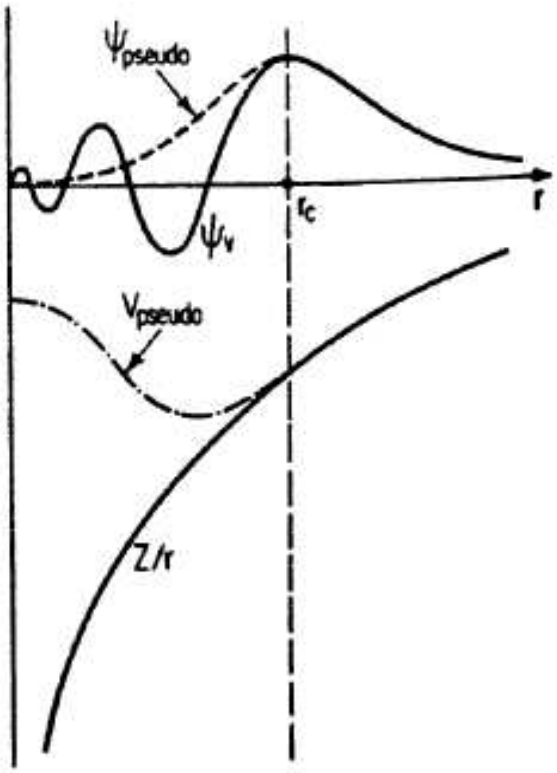

Figure 2.6 Schematic illustration of all-electron (solid lines) and pseudoelectron (dashed lines) potentials and their corresponding wavefunctions [40]

This condition has to be carefully checked for as it is possible for the pseudopotential to introduce new non-physical states (so called ghost states) into the calculation. The general form of pseudopotential is

$$V_{NL} = \sum |lm\rangle V_l \langle lm| \qquad (2.32)$$

where $|lm\rangle$ are spherical harmonics and V_l is the pseudopotential for angular momentum l

[45]. The majority of the pseudopotentials currently used in electronic structure are generated from all electron atomic calculations. However, a pseudopotential that uses the same potentials for all the angular momentum components of the wavefunction is called a local pseudopotential. The norm conserving pseudopotentials, are an example of the non-local pseudopotential, and use a different potential for each angular momentum components of the wavefunction. Local pseudopotentials are computationally much more efficient than non-local ones.

2.3.3 Norm conserving pseudopotential

If the exchange-correlation energy is to be desired accurately, the pseudo wavefunction and the real wavefunction outside the core region must be identical in both their spatial dependence and absolute magnitude for two wavefunctions to generate identical charge densities. In the attempt to construct pseudopotential of this type, Starkloff and Joannopoulos [46, 47] introduced class of local pseudopotentials that described the valance energies and wavefunctions of many heavy atoms accurately.

Generally, the non-local pseudopotential best describes the scattering from the ion core, this non-local pseudopotential uses a different potential for angular momentum component of the wavefunction. A match of pseudo and real wavefunction outside the core region also assures that the first-order energy dependence of the scattering is accurately described over a wide range of energy. Recently, Shirley et al [48] introduced a method to construct pseudopotentials that correct even the higher-order energy dependence of the scattering.

2.3.4 Ultrasoft Pseudopotentials

Vanderbilt [49] suggested a more radical approach, the ultrasoft pseudopotentials (USP). This involves relaxing the norm-conserving requirement in order to generate much "softer" pseudopotentials. In the USP scheme, the pseudo wavefunction are allowed to be as weak as possible within the core region, so that the cutoff energy can be reduced dramatically. This is achieved by introducing a generalized orthonormality condition. The electron density has to be augmented in the core region in order to recover the full electronic charge. The electron density is thus subdivided into (i) a smooth part that extends throughout the unit cell and (ii) a hard part localized in the core region. Ultrasoft pseudopotentials have another advantage besides being much softer than their norm-conserving counterparts. The generation algorithm guarantees good scattering properties over a pre-specified energy range, which results in much better transferability and accuracy of the pseudopotentials.

2.3.5 CASTEP Code

CASTEP (Cambridge Sequential Total Energy Package) [50, 51] is a software package which uses density functional theory to provide a good atomic-level description of all manner of materials and molecules. CASTEP can give information about total energies, forces and stresses on an atomic system, as well as calculating optimum geometries, band structures, optical spectra, phonon spectra and much more. It can also perform molecular dynamics simulations. In essence, however, it uses density functional theory (specifically, using planewaves and pseudopotentials) to solve approximately the Schrödinger equation

for periodic systems of atoms, yielding the total energy, atomic forces and internal stresses in the system, as well as interesting electronic properties (the electron wavefunction, charge density distribution, density of electronic states, etc.). The electronic relaxation is achieved by minimization of the total energy. This minimization is achieved using the technique called band-by-band, where each wave function is optimized independently, or by modern all band method.

CASTEP uses special k-points sampling for integration over the Brillouin zone [52, 53, 54, 55], and Fast Fourier Transforms (FFT) to evaluate matrix elements. It also uses wave function symmetrization for a crystal with point group symmetry higher than $P\bar{1}$ and for metallic systems it introduces partial occupancies for levels close to the Fermi energy. It uses both the local density approximation and the generalized gradient approximation for the exchange correlation energy functional and it also uses ultrasoft pseudopotential as put forward by Vanderbilt [49] as well as norm conserving potential.

2.3.6 VASP Code

VASP (Vienna Ab-initio Simulation Package) is a code designed to perform ab initio quantum mechanical molecular dynamics (MD) simulation using ultrasoft pseudopotentials [49] or projector-augmented wave (PAW) method [56] and a plane-wave basis set. The approach implemented in VASP is based on the (finite-temperature) [57] local density approximation with free energy as a variational quantity and an exact evaluation of the instantaneous electronic ground state at each MD time step. It uses efficient matrix

diagonalization schemes and efficient Pulay [58]/Broyden [59] charge density mixing. These techniques avoid most problems possibly occurring in the original Car-Parrinello method [60], which is based on the simultaneous integration of electronic and ionic equations of motion. The interaction between ions and electrons is described by ultrasoft Vanderbilt pseudopotentials or by the PAW method.

VASP has the same root as CASTEP/CETEP code, but branched this root at very early stage. The version of CASTEP upon which VASP is based, supported only the local pseudopotential and Car-Parrinello algorithm. In September 1991 work on VASP code started. Years later VASP was rewritten by G. Kresse and J. Furthmüller [61, 62, 63].

2.4 Theoretical Background of Calculated Properties

2.4.1 Optical Properties

Generally, the difference in the propagation of an electromagnetic wave through vacuum and some other material can be described by a complex refractive index

$$N = n + ik \tag{2.33}$$

since n is just the usual index of refraction in the regions where the crystal is non-absorbing, the velocity of propagation in a crystal, c/n (c is velocity of light in a vacuum), is slower than in a vacuum. In vacuum, N is real and equal to unity. For transparent materials it is purely real, the imaginary part being related to absorption coefficient by

$$\eta = \frac{2k\omega}{c} \tag{2.34}$$

the fraction of energy lost by the wave on passing through a unit thickness of the material concerned (ω is frequency of the incident wave and k is attenuation index). This is derived by considering the rate of production of Joule heat in the sample. The reflection coefficient can be obtained for the simple case of normal incidence on a plane surface by matching both the electric and magnetic fields at the surface,

$$R = \left|\frac{1-N}{1+N}\right|^2 = \frac{(n-1)^2 + k^2}{(n+1)^2 + k^2} \tag{2.35}$$

However, when performing calculations of optical properties it is common to evaluate the complex dielectric constant, and then express other properties in terms of it. The complex dielectric constant

$$\varepsilon = \varepsilon_1 + i\varepsilon_2 = N^2 \tag{2.36}$$

and hence the relation between the real and imaginary parts of the refractive index and dielectric constant is

$$\varepsilon_1 = n^2 - k\varepsilon_2 = 2nk \tag{2.37}$$

A further useful form for the expression of optical properties is the optical conductivity,

$$\sigma = \sigma_1 + i\sigma_2 = -i\frac{\omega}{4\pi}(\varepsilon - 1) \tag{2.38}$$

However, this is most useful for metals, which are not treated in the current study. A further property that may be calculated from the complex dielectric constant is the loss function. It describes the energy lost by a point electron passing through a homogeneous dielectric material, and is given by,

$$\mathrm{Im}\left(\frac{-1}{\varepsilon(\omega)}\right) \tag{2.39}$$

Experimentally, the most accessible optical parameters are the absorption $\eta(\omega)$, and the reflection $R(\omega)$ coefficients. In principle, given the knowledge of both, the real and the imaginary parts of *N* can be determined, through equations 2.34 and 2.35. Equation 2.36 allows expression in terms of the complex dielectric constant. However, in practice experiments are more complicated than the case of normal incidence considered above. Polarization effects must be accounted for, and the geometry can become quite involved (for example, transmission through multi-layered films or incidence at a general angle). Only transitions between properly selected bands are allowed, i.e., only the bands with the same sign of spin.

The interaction of a photon with the electrons in the system under study is described in terms of the time dependent pertubations of the ground state electronic states. Transitions are caused between occupied and unoccupied states by the electric field of the photon (the magnetic field effect is weaker by a factor υ/c). When these excitations are collective they are known as plasmons (which are most easily observed by the passing of a fast electron through the system rather than a photon, in a technique known as Electron Energy Loss Spectroscopy (EELS), described by equation 2.38, since transverse photons do not excite longitudinal plasmons). When the transitions are independent they are known as single particle excitations. The spectra resulting from these excitations can be thought of as a joint density of states (JDOS) between the valence and the conduction bands, weighted by approximate matrix elements.

2.4.2 Elasticity

Elastic properties of a solid are important because they relate to various fundamentals solid-state properties, such as equation of state, phonon spectra, etc. [64]. The elastic constant C_{ij} contains some of the more important information that can be obtained from ground-state total-energy calculations. Elastic constant for most pure metals are reported over a wide range of temperature [65, 66]. The bulk modulus is often calculated, calculations of the other elastic constant are relatively scarce [67].

The elastic constants of a material describe its response to externally applied strain or, the stress required to maintain a given deformation. For small deformations we expect a quadratic dependence of the crystal energy *E* on the strain (Hooke's law). Stress and strain have three tensile and three shear components, giving six components in total. The linear elastic constants form a 6×6 symmetric matrix, having 27 different components, such that $\sigma_i = C_{ij}\varepsilon_j$ for small stresses, σ, and strains, ε [66], where *i* and *j* are the indices attaining values from 1, 2, 3,…,6. Any symmetry in the structure can make some of these components equal, and/or some strictly zero. A cubic crystal has only three different symmetry elements (C_{11}, C_{12} and C_{44}) with each representing three equal elastic constants($C_{11} = C_{22} = C_{33}, C_{12} = C_{23} = C_{31}$ and $C_{44} = C_{55} = C_{66}$). A single strain with non-zero first and fourth components can give stresses relating to all three of these coefficients, yielding a very efficient method of obtaining elastic constant for the cubic system. Nye [68] gives a full account of the symmetry of stress, strain and elastic constant. Elasticity describes the response of a crystal under external strain and provides key information of the

strength of the material, as characterized by bulk modulus (B), shear modulus (C'), Young's modulus (E), Poisson's ratio (ν) and shear anisotropy factor (A) [64]. These elastic moduli are defined as follow:

$$B = \frac{1}{3}(C_{11} + 2C_{12}),\ C' = \frac{1}{2}(C_{11} - C_{12}),\ \nu = \frac{C_{12}}{C_{11} + C_{12}} \text{ and } A = \frac{2C_{44}}{C_{11} - C_{12}}.$$

The requirements for mechanical stability in a cubic crystal lead to the following restrictions on the elastic constants [69]:

$$C_{11} - C_{12} > 0,\ C_{11} > 0,\ C_{44} > 0,\ C_{11} + 2C_{12} > 0.$$

The single crystal shear moduli for the {100} plane along the [010] direction and for the {110} plane along the [110] direction in a cubic crystal are given by C_{44} and C', respectively. Orthorhombic deformation is related to the shear constant C_{44}, whereas the tetragonal deformation is related to C' and its size reflects the degree of stability of the crystal with respect to a tetragonal shear [70].

There are six independent elastic constants in the contracted matrix notation, C_{11}, C_{12}, C_{13}, C_{33}, C_{44} and C_{66}, for a crystal with tetragonal structure. The elastic moduli that can be derived from these elastic constant are:

$$B = \frac{1}{9}(2C_{11} + C_{33} + 4C_{13} + 2C_{12}), C' = \frac{1}{15}(2C_{11} + C_{33} - C_{12} - 2C_{13} + 6C_{44} + 3C_{66}),$$

$$E = C_{33} - 2\nu C_{13},\ \nu = \frac{C_{13}}{C_{11} + C_{12}} \text{ and } A_1 = \frac{2C_{66}}{C_{11} - C_{12}} \text{ (on basal plane),}$$

$$A_2 = \frac{4C_{44}}{C_{11} + C_{33} - 2C_{13}} \text{ (on (010) plane).}$$

The requirement for a crystal to be stable under any homogeneous elastic deformation places restrictions on the elastic constants. The stability restrictions are as follow [69]

$C_{11} - C_{12} > 0,\ C_{11} + C_{33} - 2C_{13} > 0,\ C_{11} > 0,\ C_{33} > 0,\ C_{44} > 0,\ C_{66} > 0,$

$2C_{11} + C_{33} + 2C_{12} + 4C_{13} > 0.$

A hexagonal crystal has six different symmetry elements C_{11}, C_{12}, C_{13}, C_{33}, C_{44} and C_{66}, only five of them are independent since $C_{66} = \frac{1}{2}(C_{11} - C_{12})$. The stability restrictions do not tell us anything further about the relative magnitude of various elastic constants. For polycrystalline phase as a measure of fracture or toughness in metal, Pugh [71] introduced the quotient of bulk modulus and shear modulus, B/C'. In metals and alloys behaving like isotropic media, the Young's modulus is proportional to the bulk modulus when the Poisson's ratio is close to $\frac{1}{3}$.

Chapter 3
Electronic and Structural Properties

3.1 Introduction

This chapter presents results based on ab initio calculations performed on PdS, and in particular the structural (lattice parameters, equation of state (EOS) and bond lengths), electronic (density of state and band structure) and optical properties (reflectivity and absorption). The effect of pressure on the system is discussed, particularly the equation of state (EOS), lattice parameter, density of state, reflectivity and absorption, at different pressures ranging from -10 GPa to 50 GPa. We also give a summary of the methods used. Geometry optimization calculations were performed using the computer code CASTEP, which is discussed in detail in chapter 2.

3.2 Methodology

The plane-wave pseudopotential (PWP) method is used to perform calculations on PdS structure. Plane-wave basis set is used for expanding the electronic state. The chemically inactive core electrons are replaced with ultrasoft pseudopotential [49, 72] (USP) which were obtained in the CASTEP database. To obtain accurate results, it is necessary to

perform the kinetic energy cutoff, which determines the number of plane waves in the expansion and the k-points used for the Brillouin zone integration. It is therefore imperative to ensure that appropriate energy cutoff and k-points are determined.

3.2.1 Plane-Wave Pseudopotential Method

This method is fully discussed in chapter 2 and we use it to predict the equilibrium lattice parameters, equation of state, bond lengths and internal parameters of PdS structure. In this method geometry optimization is achieved by varying the hydrostatic pressure and allowing the lattice to relax using the Broyden-Fletcher-Goldfard-Shanno (BFGS) minimization method to obtain the equilibrium geometry [73, 74, 75, 76]. Electronic minimization was performed through band-by-band conjugate gradient (CG) minimization technique.

3.2.2 Kinetic Energy Cutoff

Convergence test for the energy cutoff is important, since it determines the number of plane waves required in a calculation. Different values of energy cutoff were chosen until a constant energy was obtained, and the energy cutoff that corresponds to the minimum total energy is then used for all calculations. For PdS, the appropriate energy cutoff obtained is 500 eV. The graph of total energy versus energy cutoff is shown in figure 3.1. This cutoff energy corresponds to Fast Fourier Transformation (FFT) grid of 45×45×45 and the corresponding number of plane waves used is 7021. Pullay correction on forces was

included to compensate the energy cutoff. In all optimizations, the tolerance in total energy and pressure change before self-consistency was 2×10^{-5} eV/atom and 0.1 GPa respectively. The RMS tolerance for the atoms displacement was restricted to 0.001 Å.

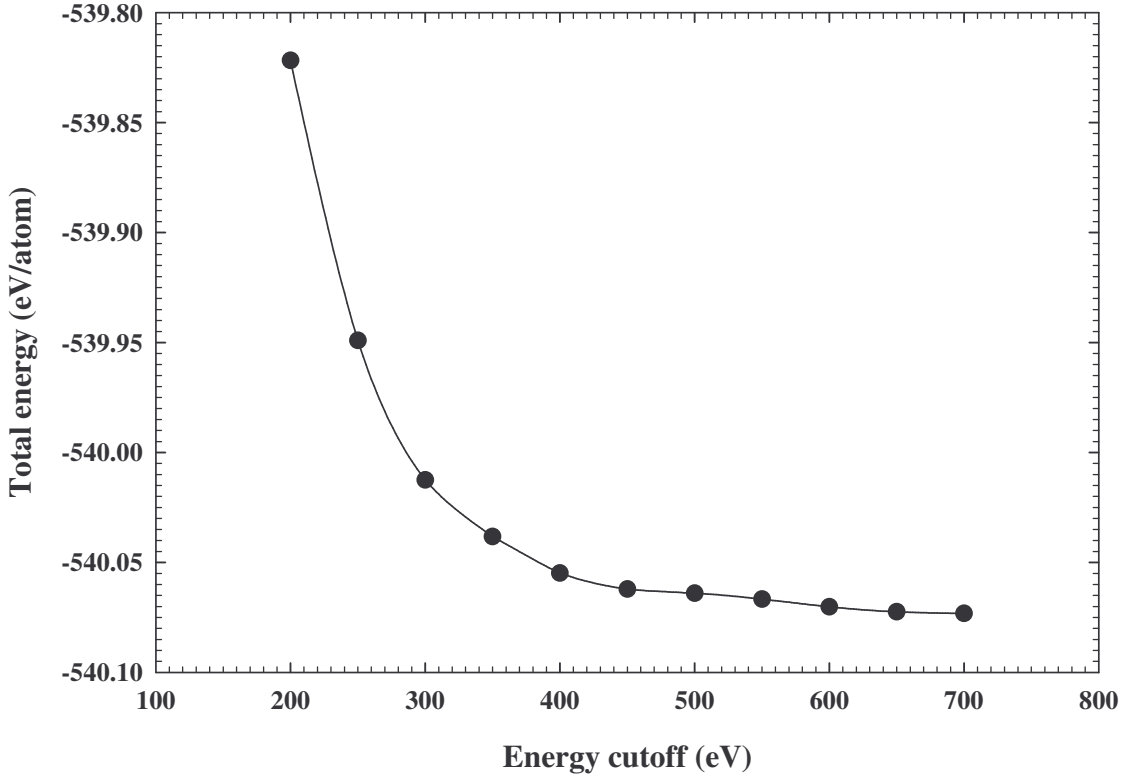

Figure 3.1 Total energy versus kinetic energy cutoff for PdS

3.2.3 K-points sampling

It is crucial for one to determine a reasonable number of k-points to use in PWP calculations for speedy convergence coupled with the accuracy of the total energy. Several methods have been suggested for special k-points sampling in the Brillouin zone [52, 53,

54, 55]. These methods help in obtaining the accurate approximation for the total energy by calculating the electronic state at a very small number of k-points.

The Monkhorst-Pack scheme of the k-points sampling was used to select an optimal set of special k-points of the Brillouin zone such that the greatest possible accuracy is achieved from the number of k-points used [24, 25]. Different values of k-points mesh parameters were varied from 3×3×3 to 8×8×8 until total energy change is within 1 meV. Our k-points mesh parameter was found to be 6×6×6 which corresponds to 27 number of k-points and figure 3.2 shows the k-points convergence of PdS

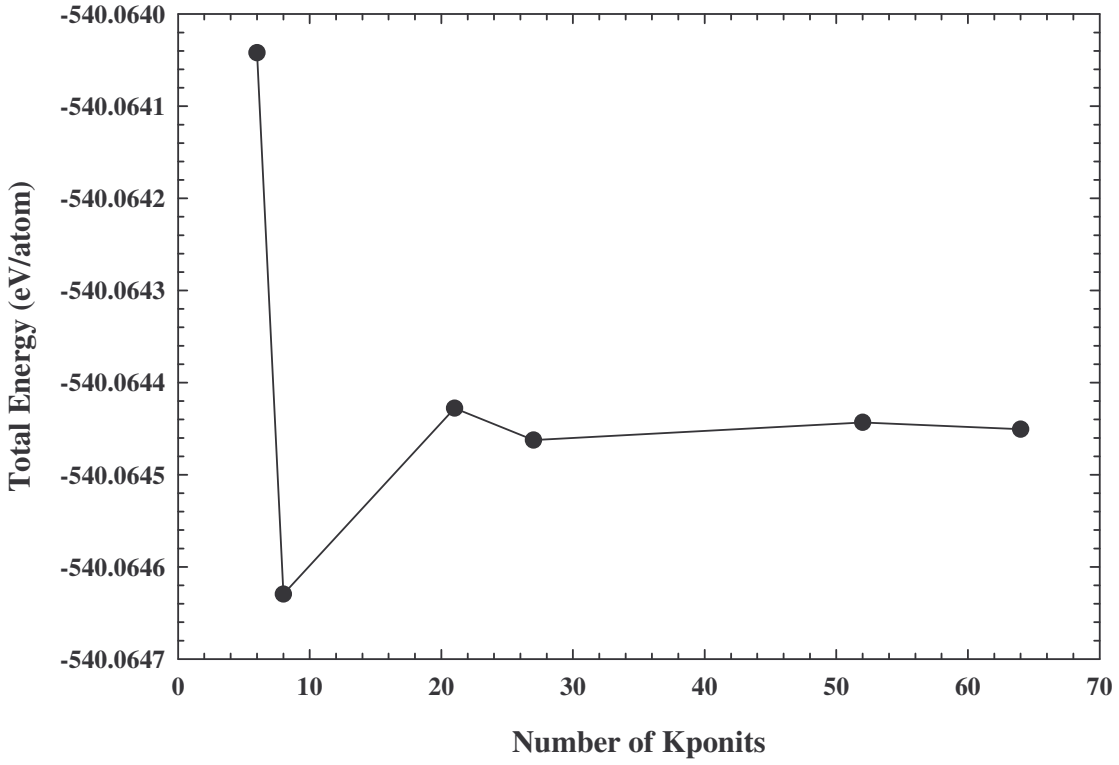

Figure 3.2 Variation of number of k-points against total energy.

3.3 Structural Properties

Geometry optimization gives the equilibrium lattice parameters and relaxed internal parameters which can be compared with experimental results. As figure 3.3 indicates, it is possible to predict the lattice parameter (volume) of a system being studied. In figure 3.3 it is apparent that the minimum of the total energy occurs at the volume of 264.1 $Å^3$ and figures 3.4 and 3.5 indicate, the minimum total energy is at lattice a = 6.350 Å and c = 6.550 Å, respectively. The deviation between the experimental results and our calculated results is 1.2%, 0.3% and 1.3% for lattice parameter a. For lattice parameter c the deviation is 0.9%, 0.2% and 1.2%, and the deviation for volume is 3.4%, 0.5% and 3.7% for Brese [10], Genkin and Zvyagintsev [12] and Gaskell [13], respectively. Table 3.1 shows the tabulated results of this calculation and the results are compared with experimental results. Comparison is again done on the volume and the axial ratio of the calculated system and the theoretical values obtained from literature (see table 3.2).

PdS was optimized at several pressures from 0 to 50 GPa enforcing its tetragonal symmetry throughout the simulation. Table 3.3 shows pressure dependence of the structural parameters of PdS. Figure 3.6 shows the decrease of lattice parameter a and c with applied pressure. The calculated pressure-volume data were fit to the third-order Birch-Murnaghan [77] equation of state (see figure 3.7). The deduced bulk modulus is B = 153.3 GPa, which will be compared to the calculated bulk modulus from VASP later in one of the following chapter 4.

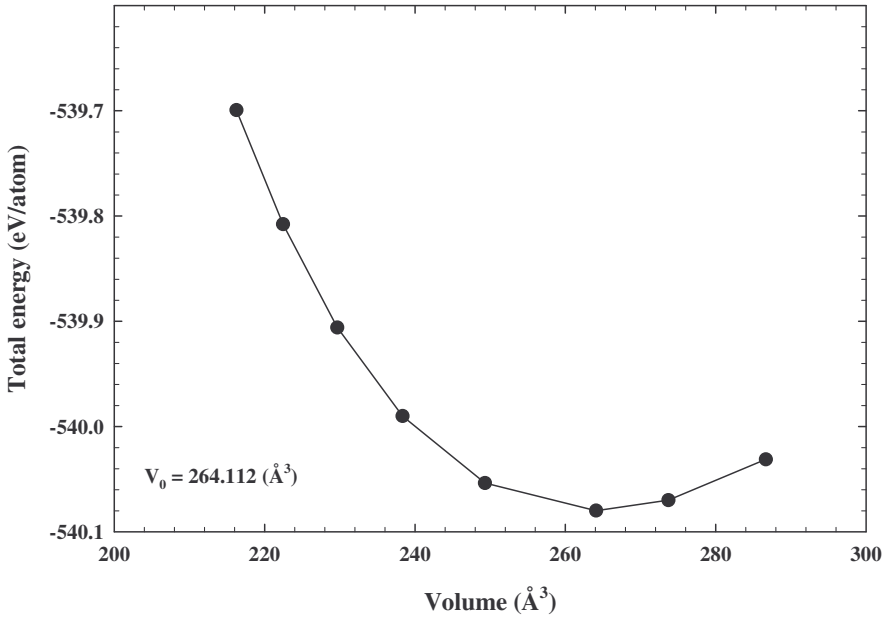

Figure 3.3 Total energy versus volume at zero pressure (0 GPa).

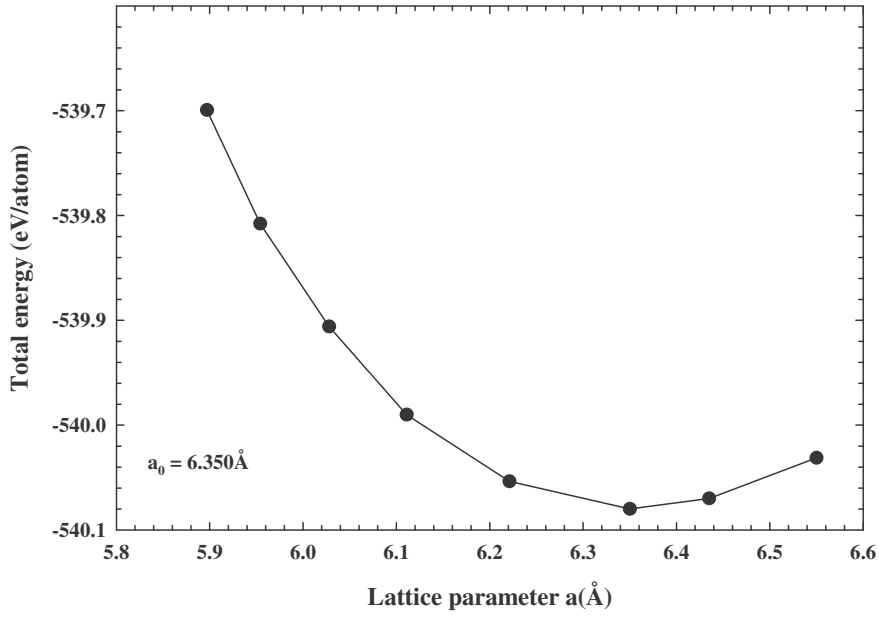

Figure 3.4 Total energy versus the *a* lattice parameter at zero pressure (0 GPa).

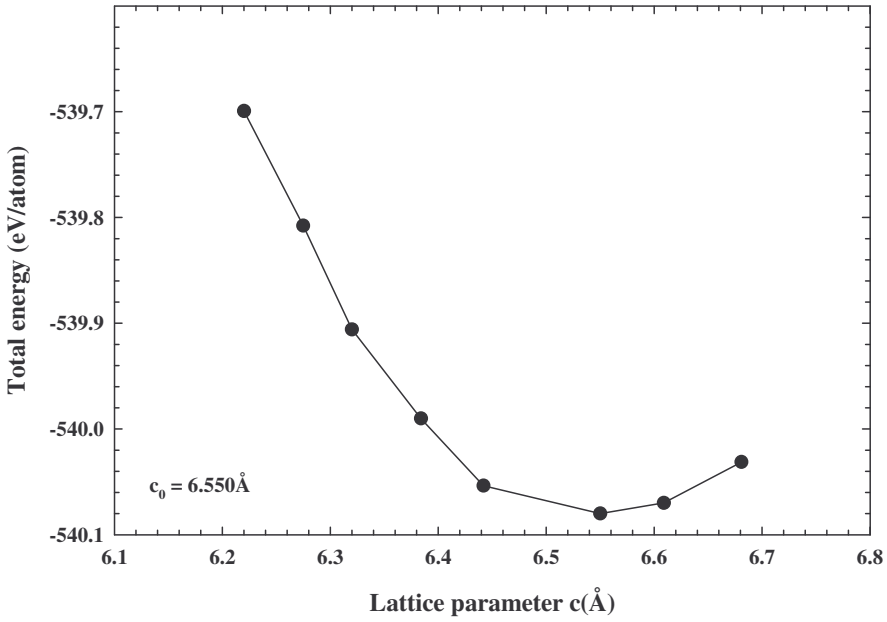

Figure 3.5 Total energy versus the c lattice parameter at zero pressure (0 GPa).

Table 3.1 Calculated and experimental structural parameters of PdS.

	a (Å)	c (Å)	V (Å^3)
Calc. (This work)	6.350	6.550	264.112
Expt. [10]	6.429	6.611	273.246
Expt. [12]	6.371	6.540	265.456
Expt. [13]	6.430	6.630	274.117

Table 3.2 Comparison of present and previous calculated structural parameters of PdS.

	V_{LDA}/V_{exp}	V_{GGA}/V_{exp}	$(c/a)_{exp}$	$(c/a)_{GGA}$	$(c/a)_{LDA}$
Calc. (This work)	0.97	-		-	1.03
Calc. (Pseudopotential) [11]	0.97	1.04	1.03	1.03	1.04

Currently, there is no experimental value for bulk modulus of PdS available in literature. The one dimensional analog of the Murnaghan equation provides an approximation for

describing the nonlinear relation between normalized lattice parameters and pressure P,

$$\frac{r}{r_0} = \left[\left(\frac{B'}{B_0}\right)P + 1\right]^{-\frac{1}{B'}} \tag{3.1}$$

where, r is the lattice constant along one of the crystal axes, $k = B_0^{-1} = -\left(\frac{\partial \ln r}{\partial P}\right)_{P=0}$ is the linear compressibility, and B´ is the pressure derivative of B (i.e. $\frac{\partial B}{\partial P}$). The compressibility along the c-axis is defined as

$$k_c = \frac{1}{c_0}\left(\frac{\partial c}{\partial P}\right)_{P=0} \tag{3.2}$$

Here, c is the c-axis lattice constant and c_0 is the c-axis lattice constant at pressure P_0.

Table 3.3 Pressure dependence of the structural parameters of PdS

Pressure (GPa)	a (Å)	a/a_0	c (Å)	c/c_0	a/c	V (Å^3)	V/V_0
0	6.350	1	6.550	1	1.031	264.112	1
10	6.221	0.980	6.442	0.984	1.036	249.311	0.944
20	6.111	0.962	6.384	0.975	1.045	238.359	0.903
30	6.028	0.949	6.320	0.965	1.048	229.675	0.870
40	5.954	0.938	6.275	0.958	1.054	222.455	0.842
50	5.897	0.929	6.220	0.950	1.055	216.256	0.819

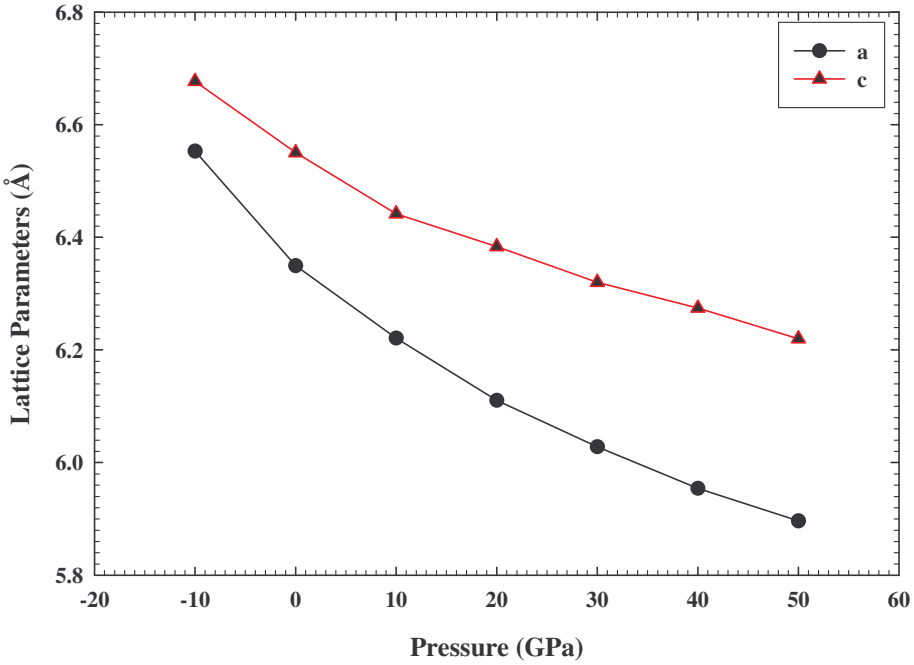

Figure 3.6 Lattice constants for PdS as a function of pressure

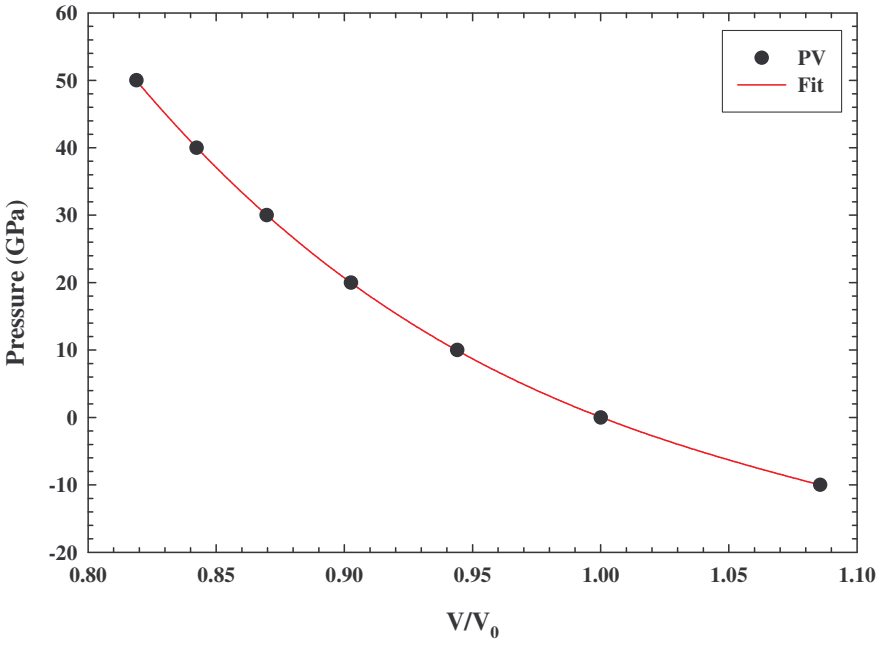

Figure 3.7 The calculated equation of state for PdS. The black circle represents the calculated values and the red solid line represents the curve fit.

The pressure variations of the normalized lattice parameters a/a_0, c/c_0 and a/c were computed, and are displayed in figure 3.8. They are observed to be decreasing with increasing pressure and the parameter a/c, which increases with pressure. The relative lattice constants are plotted and fitted to the Murnaghan equation of state from which we obtain the bulk moduli B_a, B_c the derivative of the bulk moduli (B_a' and B_c') at ambient pressure (0 GPa) and the compressibility (k_a and k_c). The results are shown in table 3.4 and are compared with the calculated value of braggite ($PdPt_3S_4$) since they have the same crystal structure, symmetry and space group. The calculated and experimental bond lengths of PdS at ambient pressure (0 GPa) are shown in table 3.5, and compare reasonably.

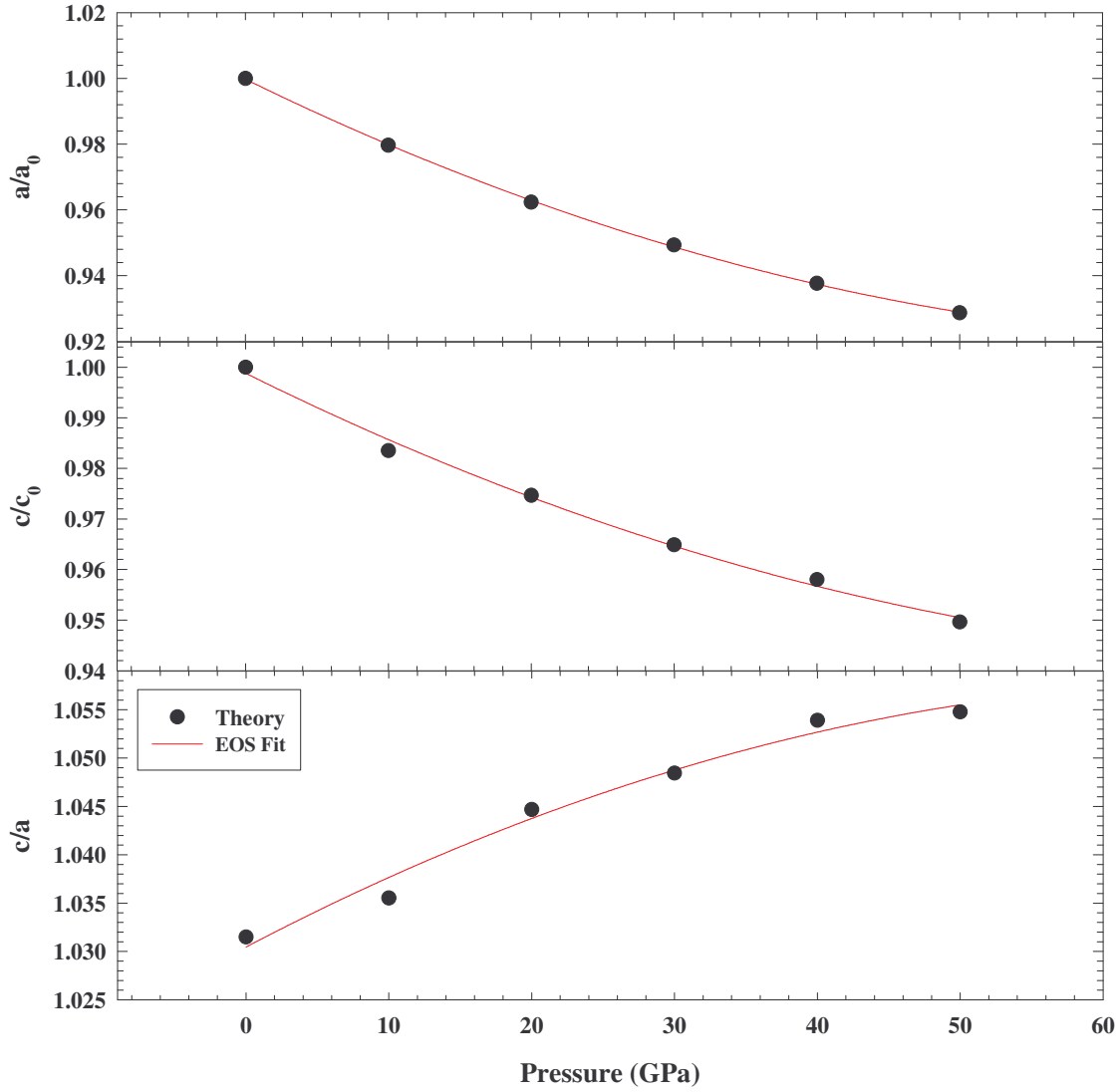

Figure 3.8 The relative lattice constant a/a_0, c/c_0 and a/c of PdS as a function of pressure.

Table 3.4 First-and-second-order axial compression coefficients of PdS calculated using USP pseudopotentials, compared with those of braggite.

	B_a GPa	B_c GPa	B_a'	B_c'	k_a 10^{-3}GPa^{-1}	k_c 10^{-3}GPa^{-1}
Calc. (This work)	409.64	586.60	12.51	19.14	2.44	1.71
Calc. [78]	370.30	874.77	16.20	12.80	2.70	1.14

Table 3.5 Calculated and experimental bond lengths of PdS at equilibrium volume

Bond Length (Å)	Calc.	Expt. [10]
Pd(1)-4S(1)	2.313	2.341
Pd(2)-4S(1)	2.294	2.318
Pd(3)-2S(1)	2.309	2.337
Pd(3)-2S(1)	2.325	2.346
Pd(3)-Pd(3)	3.089	3.150
Pd(1)-2Pd(1)	3.281	3.306
Pd(1)-4Pd(2)	3.572	3.615
Pd(1)-4Pd(3)	3.788	3.809
Pd(2)-2Pd(3)	3.361	3.389
Pd(2)-4Pd(3)	3.671	3.702
Pd(3)-4Pd(3)	3.942	3.986
Pd(1)-4Pd(3)	4.081	4.144
S(1)-S(1)	2.995	3.029
S(1)-2S(1)	3.255	3.302
S(1)-2S(1)	3.272	3.316
S(1)-S(1)	3.566	3.510

3.4 Electronic Properties

3.4.1 Density of States

The density of states (DOS) shows the contribution of states from palladium (Pd) and sulphur (S) atoms, and these contributions are analyzed from the partial density of states. The total DOS of PdS is the contribution of both the Pd-states and S-states; hence it is

important to understand the way electrons are allocated for individual atoms in the system. Figure 3.9 gives the total (DOS) and the partial density of states (PDOS) of PdS. The calculations were carried out at fully relaxed atomic positions and unit cell parameters. At ambient pressure 0 GPa, PdS has an indirect band gap of 0.6 eV which is in agreement with other measured energy gaps, which range from 0.02 eV to 2 eV [4, 7, 9]. Folmer et al. [5] reports the upper limit for PdS band gap as 2 eV, since the photoresponse of the lock-in amplifier decreased to the noise level at approximately 2 eV.

The valance part of the DOS consists of three isolated peaks positioned from -14.3 eV to -12.2 eV, and a broader distribution extending from -7 eV up to the valance band maximum (VBM). The lower part of the conduction band consists of a continuous distribution of states. The partial density of states shown in figure 3.9 sheds useful insights. Three peaks ranging from -14.3 eV to -12.2 eV correspond mainly to the S (3s) states. The broader distribution between -7 eV and VBM emanate predominantly from the S(3p) and Pd(4d) states. In the conduction band, the peaks from 0.6 eV to 3.2 eV correspond to the S(3p) and the Pd(4d) states. A continuous distribution of peaks is noted from the Pd(4s and 4p) and a small contribution of the S(3p) states. In figure 3.10 the density of states of PdS were studied under hydrostatic pressure and the actual size of the band gap remains constant, whilst the peaks just below and above the Fermi energy move to the left and to the right respectively. Even though PdS and $PdPt_3S_4$ have the same crystal structure, symmetry and space group, the behaviour of the band gap differs. The band gap of $PdPt_3S_4$ increases with increasing pressure [78].

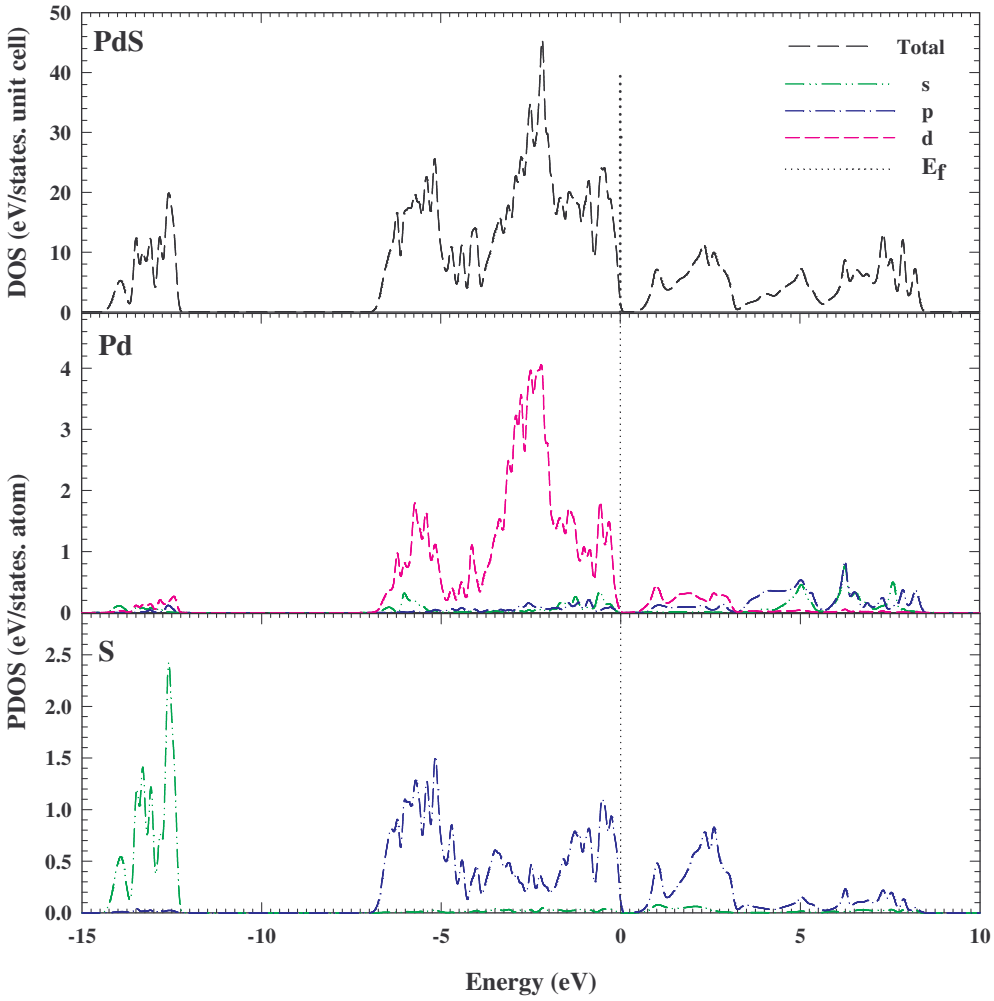

Figure 3.9 Total and partial density of states of PdS at zero pressure (0 GPa).

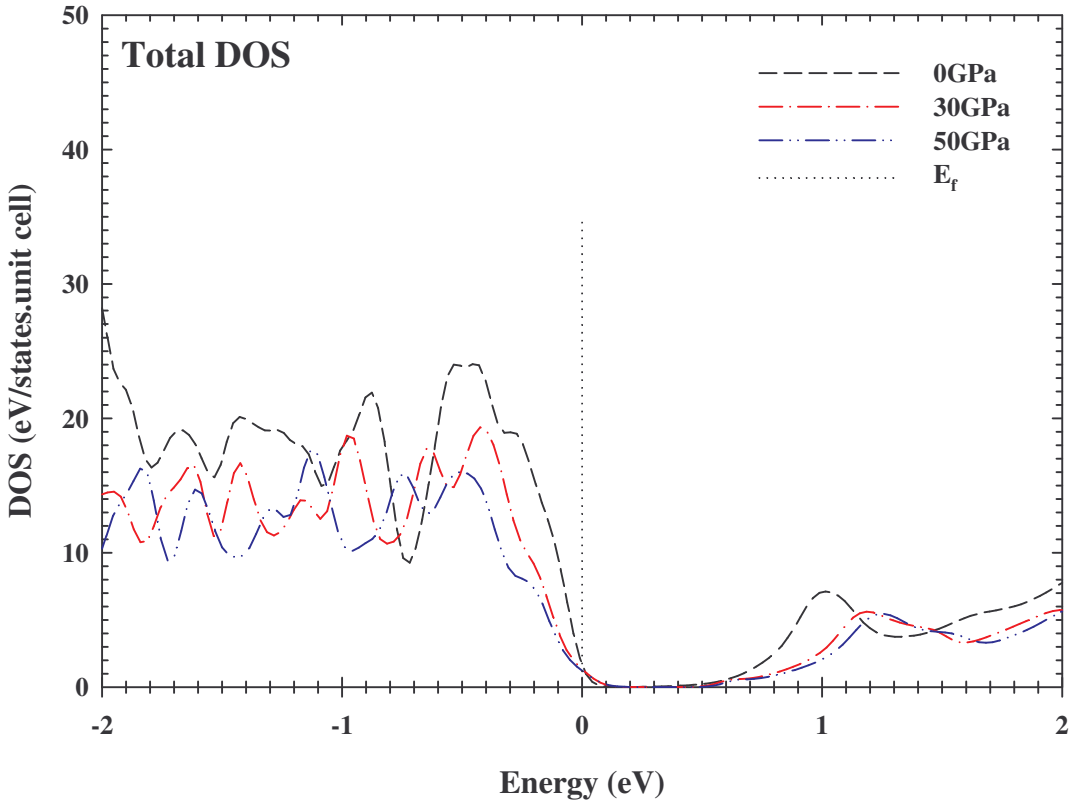

Figure 3.10 Total density of states of PdS projected around the Fermi energy at different pressures (0, 30, 50GPa).

3.4.2 Charge Density Difference

The charge density differences are of immense interest since they depict the nature of bonding between palladium (Pd) and sulphur (S) atoms. They are calculated from the charge density differences by subtracting pseudocharge distributions for individual atoms from that of a compound. Figure 3.11, shows the charge density differences of PdS at pressure 0 GPa and 50 GPa, respectively on the (0 0 1) slice. The red colour in this figure indicates a charge gain, green shows a neutral region between the atoms whilst the blue

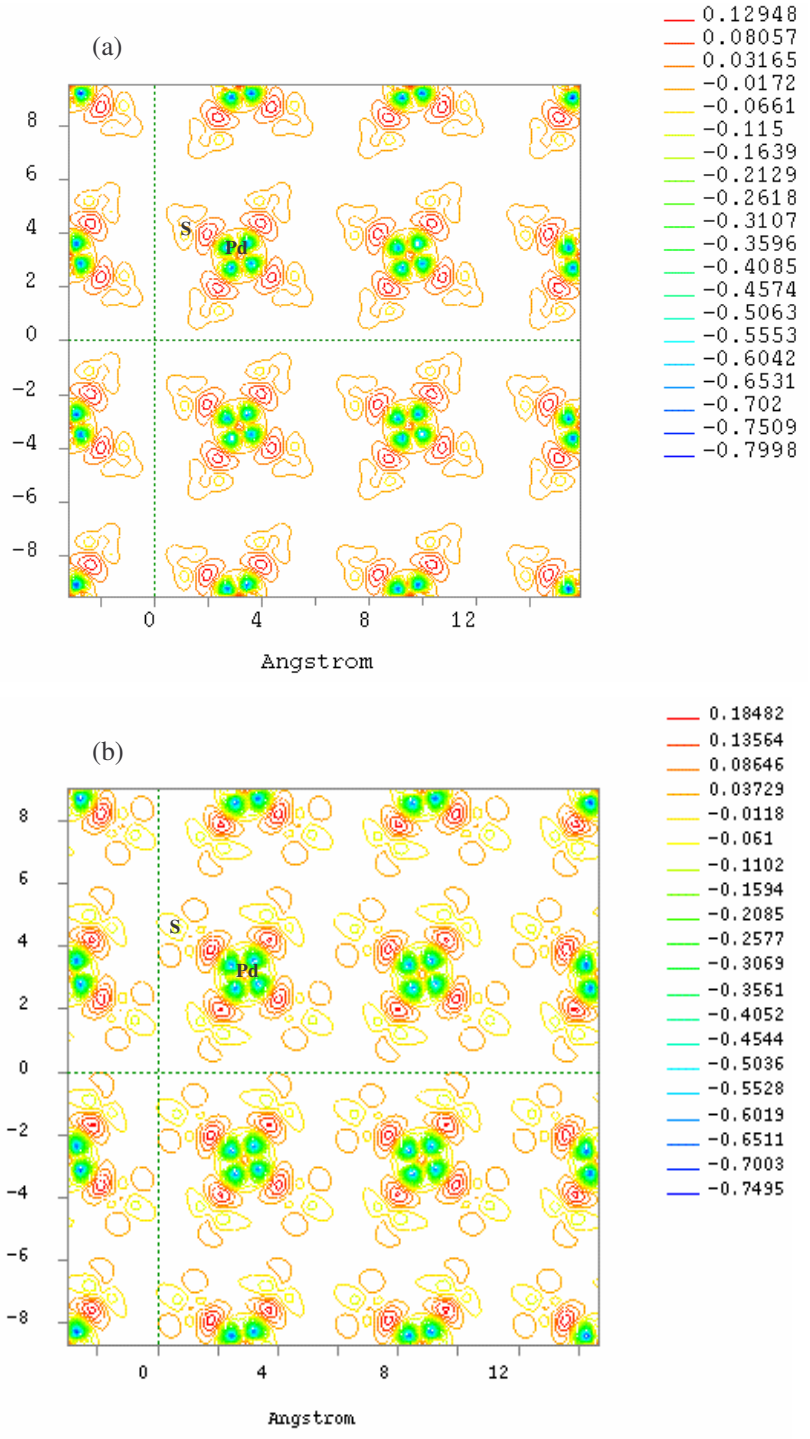

Figure 3.11 The electronic charge density differences of PdS determined at (a) 0 GPa and (b) 50 GPa. The red colour indicates a charge gain, green shows a neutral region between the atoms whilst the blue colour depicts the charge loss.

colour signifies the charge loss. Upon analysis of Pd-Pd, Pd-S and S-S bondings, at 0 GPa, it is evident that high concentration of charge is located between Pd and S atoms, hence reflecting covalent bonding. The Pd-Pd and S-S interactions are minimal. However at 50 GPa, the sharing of charge between S atoms appears to be emerging.

3.5 Optical Properties

In chapter 2, under section 2.4 we have explained in detail the method for calculating the optical properties. Our calculations are based on the Kohn-Sham DFT eigenvalues. However the exact Kohn-Sham DFT does not provide direct information on excitation energies and any calculation of optical properties based on Kohn-Sham DFT is only a first order approximation. We used the norm conserving potentials, with a cutoff of 800 eV within the CASTEP code. Reflectance spectra of PdS, under different pressures are shown in figure 3.12. Reflectance is the easiest optical property to measure experimentally, but in most cases reflectance (R) is rather a slow varying function of wavelength and this makes it very difficult to locate the exact energies of interband transitions. The reflectance spectrum of PdS at ambient pressure shows a maximum reflectance peak of magnitude 0.39 at 2 eV. A noticeable reduction of this reflectance peak and its shift to the right is observed as pressure increases. Above 5 eV most distinct peaks are enhanced in magnitude and are displayed to higher energies with increasing pressure.

The absorption spectra of PdS under high pressure are shown in figure 3.13. In view of the band gap, semiconductors are unable to absorb and reflect lower energies. Absorption and

reflection start to occur at frequency ω_0, given by $\hbar^2\omega_0 = E_g$, and at this frequency we notice the so-called absorption edge. The absorption edge is responsible for the width of the band gap. The absorption of PdS was calculated up to 30 eV. We observe the main spectral absorption at around 3.5, 11, 15 and 17 eV. There could also be transitions between the valence and the conduction band (intraband transitions) for both occupied and unoccupied orbitals. The calculated absorption edge commences at 0.6 eV, which is comparable to the energy gap of 0.6 eV determined by density of states (DOS). We also observe a decrease in the intensity of the peak at lower energy but rapid increment at higher energies as pressure increases. Absorption is enhanced under pressure, and spectral features are shifted to higher energies.

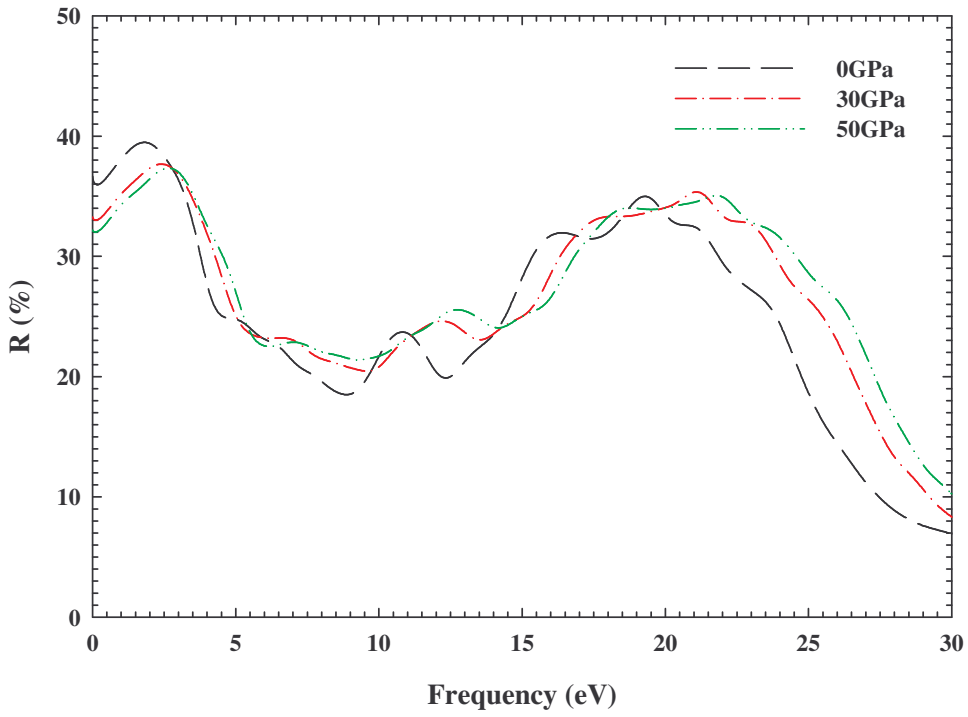

Figure 3.12 The calculated reflectivity spectra of PdS at different pressures.

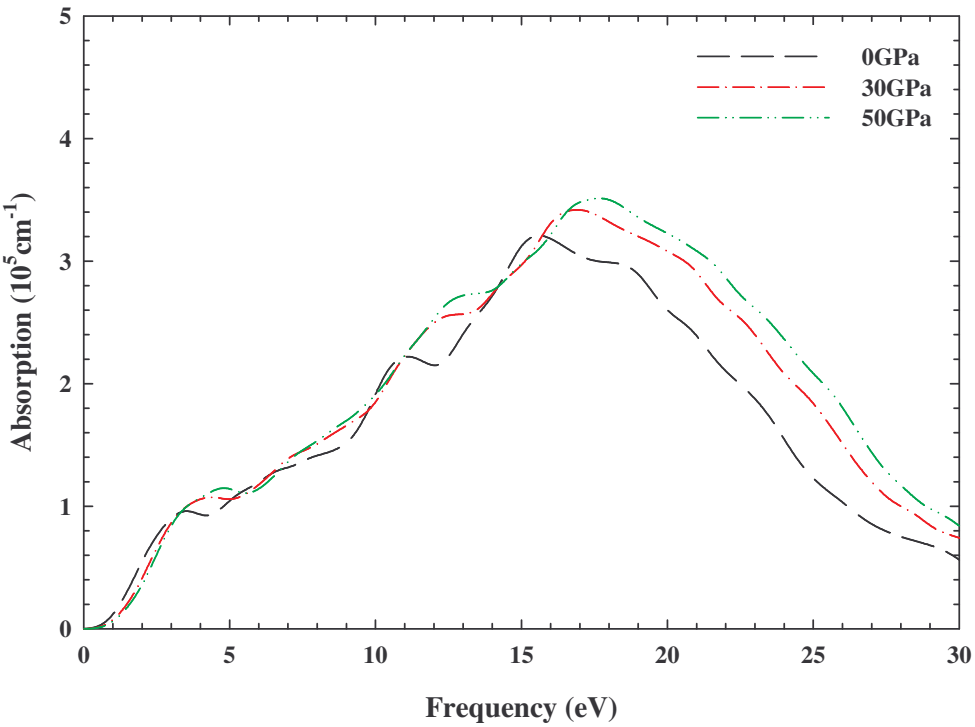

Figure 3.13 The calculated absorption spectra of PdS at different pressures

3.5.1 Comparison with the experiments

Figure 3.14 shows calculated reflectance spectra of PdS, platinum (Pt) and nickel (Ni) ternaries along with the experimental results of Criddle and Stanley [1]. The measurements were done within the visible region ranging from 400 nm to 700 nm. At lower energy range, where the measurement of reflectivity is direct and band structure underlying the calculation is more accurate, the calculated reflectivity of PdS (vysotskite) is more than 44.4 % at 400 nm as compared to 42 % of experimental value, which is a deviation of approximately 5.6 % but at 700 nm the deviation between the calculated and experimental

value is approximately 2.6 %. The difference can be attributed to their compositional variation, since the PdS sample contains fractions of platinum and nickel, whereas our model has neither traces of platinum (Pt) nor nickel (Ni). However, the shape of the calculated reflectance curve resembles the experimental measurements. The reflectivity increases between 400 nm and 600 nm and tends to a constant value beyond this range. In order to investigate if compositional variation and atom positions affect our reflectance, we calculated the reflectivity of $Pd_{4-x}Pt_xS_4$ and $Pd_{4-x}Ni_xS_4$. When investigating the effect of atom positions, atom Pd(1) with atomic position 2a is replaced with Pt or Ni and we name the structure Pd_3PtS_4_Pt or Pd_3NiS_4_Ni for nickel; when Pd(2) with atomic position 2e is replaced with Pt or Ni the structure is labeled Pd_3PtS_4_Pd or Pd_3NiS_4_Pd.

In figure 3.14, we observe that, when we have 25 % of platinum (Pt) for the system Pd_3PtS_4_Pt the reflectance spectrum reduces to 43.4 % at 400 nm. It then becomes equivalent to the experimental spectrum between 540 and 570 nm, however, between 590 nm and 680 nm the reflectance deviates by approximately 0.2 % and above 680 nm the spectrum tends to the experimental curve. For the system Pd_3PtS_4_Pd the reflectance reduces to 41.4 %, and increases towards the experimental values between 420 and 660 nm, but above 660 nm the spectrum reverts to the experimental curve. Hence the position of atoms in the unit cell affects the magnitude of reflectance considerably. With 25 % of nickel (Ni) in the system Pd_3NiS_4_Ni, the reflectance reduces to 42.4 % at 400 nm which is equivalent to that of the experimental spectrum. However between 430 and 660 nm the reflectance is below the experimental value by 0.6 %, and becomes equivalent to the spectrum of Pd_3PtS_4_Pt between 630 and 690 nm, both spectra are nearly equivalent to the

experimental PdS spectrum between 680 and 700 nm. In regard to Pd_3NiS_4_Pd, the reflectance increases to 44.6 % at 400 nm and 48.8 % at 700 nm. We generally note that locating Pt and Ni at 2a position in the PdS unit cell, yields a good agreement between the calculated and experimental reflectance, whereas the 2e position introduces significant deviations. Such agreements suggests the presence of Pt and Ni in the samples that were used in measurements, and further proposes where these impurities are likely to be located in the unit cell.

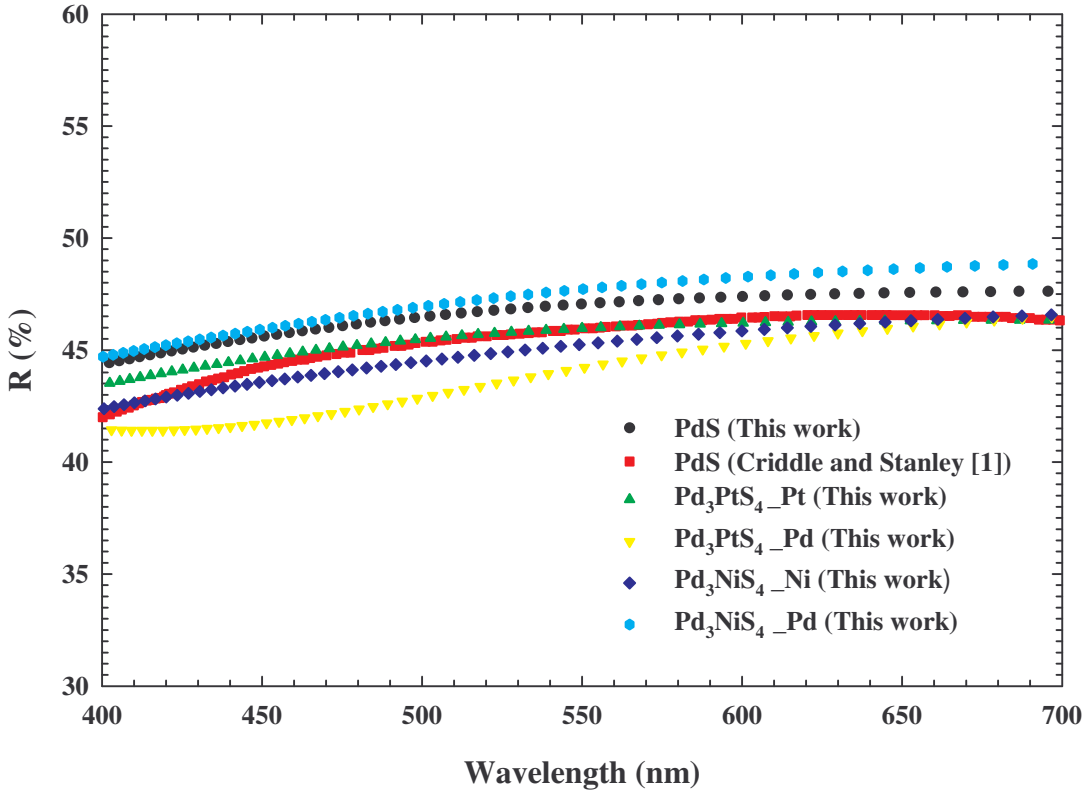

Figure 3.14 Comparison of calculated reflectivity of $Pd_{4-x}Pt_xS_4$ and $Pd_{4-x}Ni_xS_4$ with experimental result.

Figure 3.15 shows the calculated absorption coefficient of PdS along with the experimental

results of Ferrer et al. [4]. Ferrer observed values of absorption coefficient (α) higher than 2.0×10^5 cm^{-1} at $hv > 2.0$ eV, but at we observe values of α higher than 0.6×10^5 cm^{-1} at $hv > 2.0$ eV but less that 1.3×10^5 cm^{-1} at 3.0 eV. Although these magnitudes are different, the shape of the calculated absorption coefficient curve nearly resembles the experimental measurement.

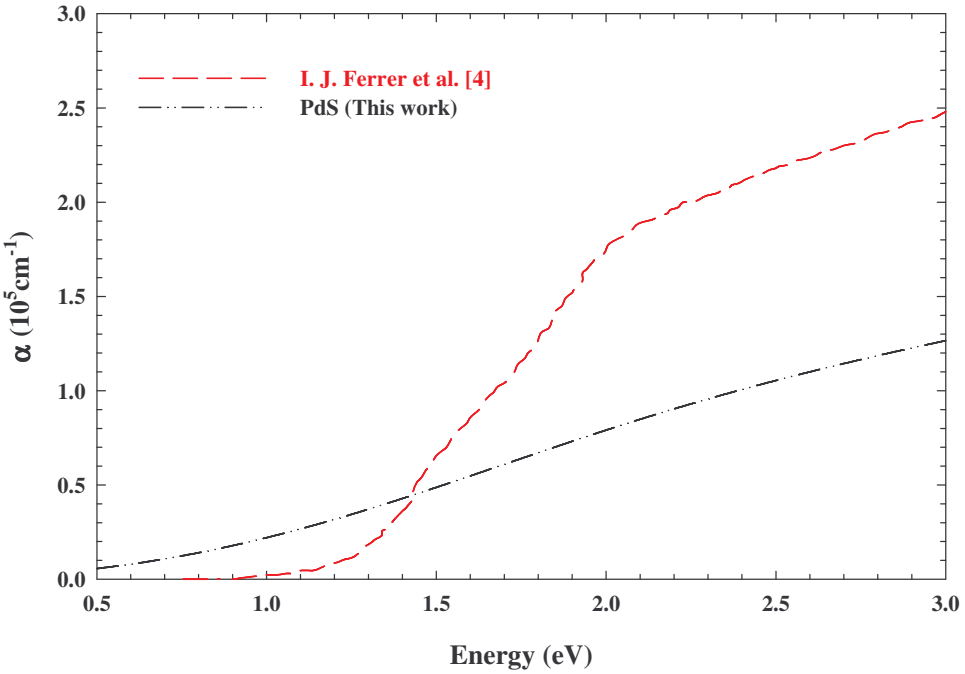

Figure 3.15 Calculated and experimental optical absorption coefficient of PdS.

Chapter 4

Miscibility Gap

4.1 Introduction

In this chapter, we discuss a possibility of miscibility gap between cooperite, braggite and vysotskite. Recently experimental investigations of the PtS-PdS-NiS system [79, 80] confirmed the presence of miscibility gap between cooperite and braggite and a continuous solid solution series between braggite and vysotskite. Contrary to the experimentally confirmed miscibility gap between cooperite and braggite, a compilation of analyses reported in the literature from worldwide occurrences [81] seems to imply a continuum of compositions between vysotskite and cooperite with no obvious gap as shown in figure 4.1. We study the stability of binary and ternary compounds from PtS to PdS by investigating the heats of formation, elasticity and electronic properties (especially pseudogap). Consequent results are then discussed and correlated to the stability of binary to ternary compounds from PdS to PtS, which in turn will help us understand if a miscibility gap between these compounds exists.

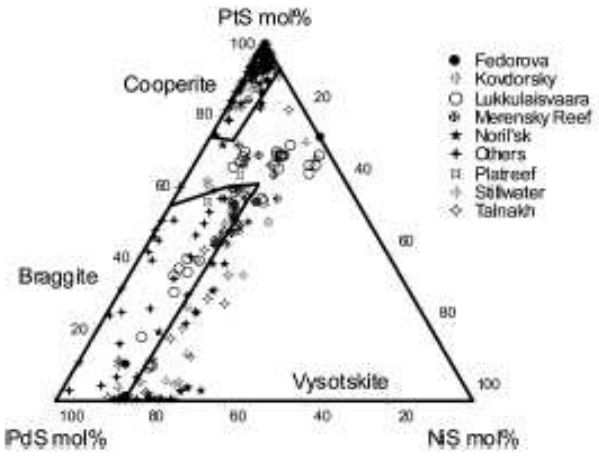

Figure 4.1 Compilation of analyses reported in the literature from worldwide occurrences [81].

4.1 Concentrations

Since PdS has three distinct sublattices of Pd, we generated five different concentrations of Pd and Pt from this structure. The common thing about these structures is that, they have the same symmetry. In order to obtain different concentrations we had to change certain atoms from Pd to Pt. We also used the PtS structure in our study, which has only one Pt sublattice. From PtS structure, we managed to generate two different concentrations, that is pure PdS and PtS which have different symmetries from ternary. All structures are shown in figure 4.2.

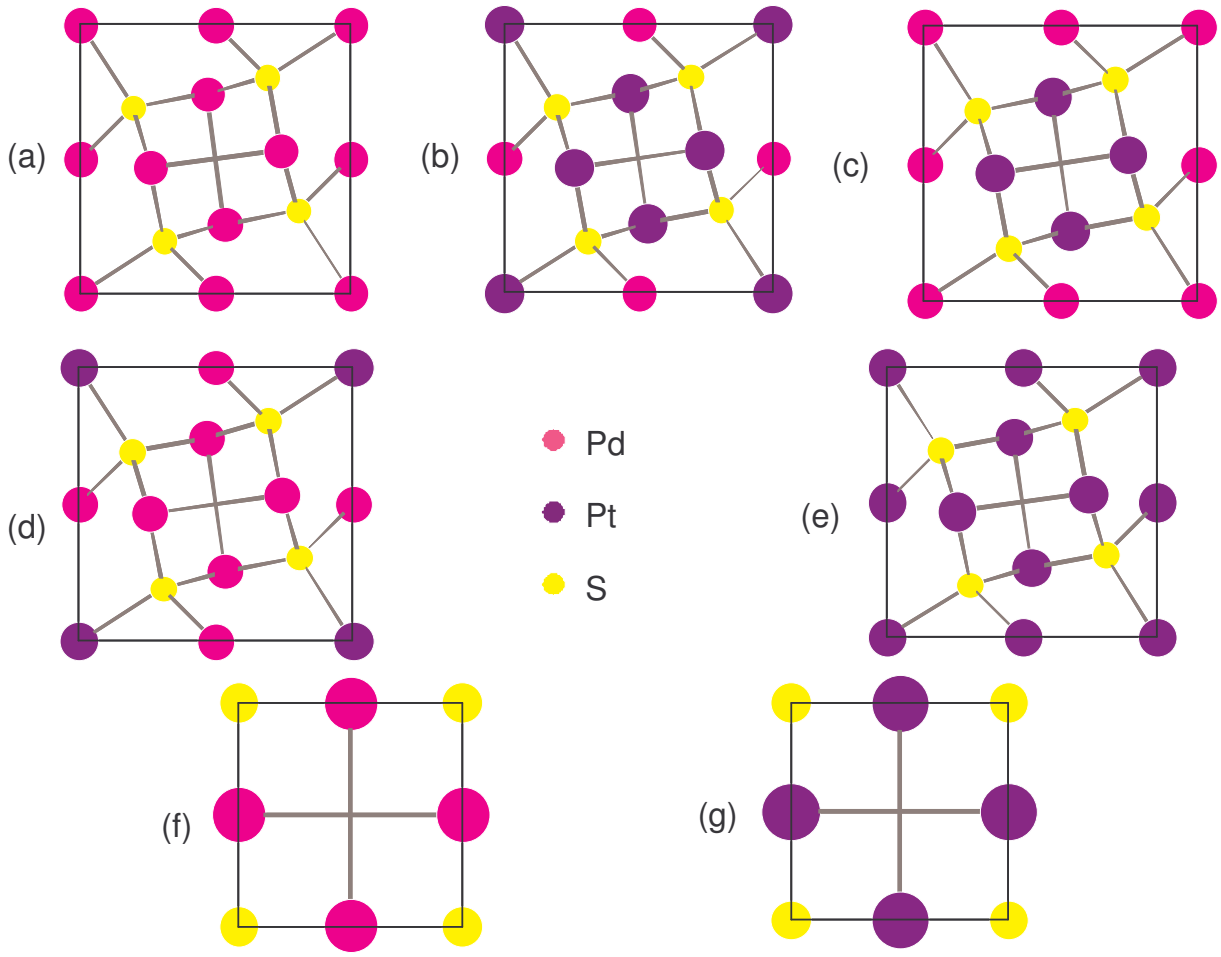

Figure 4.2 Structures with PdS symmetry but different concentrations of Pd and Pt (a) 100% Pd (PdS), (b) 25% Pd ($PdPt_3S_4$), (c) 50% Pd ($Pd_2Pt_2S_4$), (d) 75% Pd (Pd_3PtS_4) and (e) 0% Pd (PtS). We also have two structures with PtS symmetry (f) 100% Pd and (g) 100% Pt).

4.3 Stability

4.3.1 Elastic Properties

A given crystal cannot exist in a stable or metastable phase unless its elastic constant C_{ij} obeys certain relationships. Elastic constants also determine the response of a crystal to external forces and play an important role in determining the strength of the material. The C_{ij} can also be used to check phase stability of proposed compounds [83, 84]. First-principles calculations that use periodic boundary conditions assume the existence of a single crystal; hence all elastic constants can be determined by direct computations.

We calculated elastic moduli of binary and ternary compounds from PtS to PdS using the VASP code. Practically, elastic coefficients from first-principle methods are determined by setting either the stress or the strain to a small finite value, optimize any free parameters of the structure, and calculate the strain or stress. With a careful choice of the applied deformations, the elastic moduli can be determined. The elastic properties were calculated using the method developed by Nielsen and Martin [85]. In section 2.4, we discussed the criteria that have to be satisfied by elastic constants for compounds to be stable. We first present the structural parameters of these compounds (see table 4.1) which were calculated by VASP code using LDA and ultrasoft pseudopotentials. The calculated structural parameters compare well with experimental results. The calculated elastic properties of binary and ternary compounds from PtS to PdS are displayed in table 4.2.

Table 4.1 Calculated and experimental structural parameters of binary and ternary compounds, from PtS to PdS.

Compounds	Concentration (% Pd)	Space group	Calc.		Exp.	
			a (Å)	*c* (Å)	*a* (Å)	*c* (Å)
PtS	0	P42/m	6.380	6.566	-	-
$PdPt_3S_4$	25	P42/m	6.370	6.563	6.370[a]	6.540[a]
$Pd_2Pt_2S_4$	50	P42/m	6.375	6.571	-	-
Pd_3PtS_4	75	P42/m	6.391	6.538	-	-
PdS	100	P42/m	6.381	6.565	6.429[b]	6.611[b]
PtS	0	P42/mmc	3.450	6.091	3.470[c]	6.110[c]
PdS	100	P42/mmc	3.445	6.122	-	-

[a] Childs and Hall [15]
[b] N. E. Brese et al. [10]
[c] D. J. Vaughan et al. [86]

Table 4.2 Calculated elastic constants of binary and ternary compounds from PtS to PdS.

Compounds	Concentration (% Pd)	Space group	C_{11} GPa	C_{12} GPa	C_{13} GPa	C_{33} GPa	C_{44} GPa	C_{66} GPa
PtS	0	P42/m	237.50	142.20	132.35	274.80	48.80	64.40
$PdPt_3S_4$	25	P42/m	232.70	139.00	130.90	266.70	41.80	56.80
$Pd_2Pt_2S_4$	50	P42/m	207.20	133.30	122.40	260.70	37.00	53.00
Pd_3PtS_4	75	P42/m	210.80	120.00	118.00	233.30	31.60	45.60
PdS	100	P42/m	185.00	119.70	113.65	215.80	22.40	38.60
PtS	0	P42/mmc	211.20	72.30	146.65	339.60	29.00	12.00
PdS	100	P42/mmc	159.70	61.70	122.60	266.20	12.40	6.80

All compounds meet the requirements for a crystal to be stable under any homogeneous elastic deformation, the requirements are as follow $C_{11} - C_{12} > 0$, $C_{11} + C_{33} - 2C_{13} > 0$, $C_{11} > 0$, $C_{33} > 0$, $C_{44} > 0$, $C_{66} > 0$, $2C_{11} + C_{33} + 2C_{12} + 4C_{13} > 0$. Figure 4.3 shows the variation of elastic constants of $Pd_{4-x}Pt_xS_4$ with Pd content. We generally notice a decrease

in all elastic constants as the Pd concentration increases. In the case of C_{11}, we observe a departure from linearity and a fluctuating trend between 25% and 100% Pd concentration. C_{12} and C_{33}, reflect constant decrease from 0% to 50% followed by a steeper reduction from 50% to 100% Pd concentration. On the contrary C_{12} depicts a reduced slope above 50% Pd concentration. A linear decrease of C_{44} and C_{66} occurs as Pd content is increased.

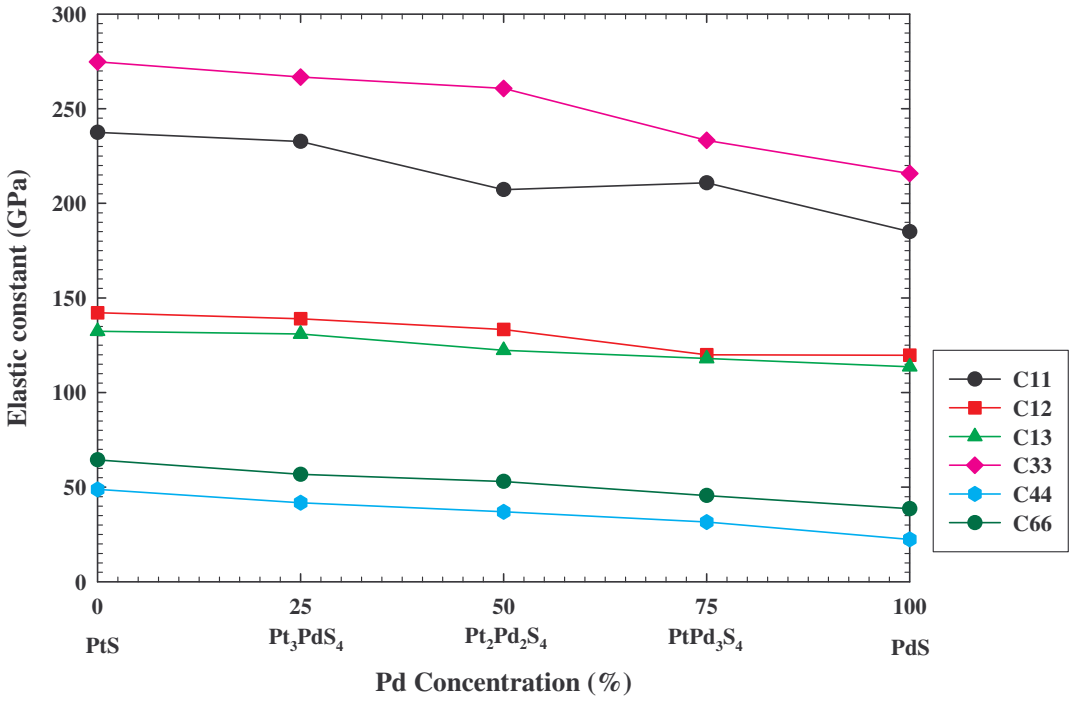

Figure 4.3 Variation of elastic constants of $Pd_{4-x}Pt_xS_4$ versus Pd concentration.

The calculated bulk, shear and Young's moduli of $Pd_{4-x}Pt_xS_4$ are presented in table 4.3. PtS, with vysotskite structure, has the highest bulk, shear and Young's moduli. It can therefore

be summarized that PtS (P42/m) is much harder than all other concentrations, with the trend of the hardness suggested as: PtS (P42/m) > $PdPt_3S_4$ (P42/m) > PtS (P42/mmc) > $Pd_2Pt_2S_4$ (P42/m) > Pd_3PtS_4 (P42/m) > PdS (P42/m) > PdS (P42/mmc). Our calculated bulk moduli are comparable with those obtained by Ntoahae [78]. Figure 4.4 shows the variation of different calculated moduli with Pd concentration. We note that as Pd concentration increases, the moduli decrease. The moduli vary linearly with Pd concentration up to 50%, and slopes change above this concentration.

Table 4.3 Bulk, shear and Young's modulus for binary and ternary compounds from PtS to PdS.

Compounds	PtS	$PdPt_3S_4$	$Pd_2Pt_2S_4$	Pd_3PtS_4	PdS	PtS	PdS
Concentration (%Pd)	0%	25%	50%	75%	100%	0%	100%
Space group	P42/m	P42/m	P42/m	P42/m	P42/m	P42/mmc	P42/mmc
				Bulk modulus (GPa)			
Voigt	173.73	170.41	159.03	151.88	142.20	165.91	133.27
Reuss	173.31	170.02	157.95	151.59	141.72	141.62	109.62
Hill	173.52	170.22	158.49	151.73	141.92	153.77	121.45
Calc.	-	184.22[a]	-	-	153.29[b]	141.12[a]	-
				Shear modulus (GPa)			
Voigt	55.26	50.17	45.20	41.69	32.60	40.43	24.90
Reuss	49.12	43.98	38.05	37.00	27.77	26.96	14.01
Hill	52.22	47.07	41.62	39.34	30.19	33.69	19.45
				Young's modulus (GPa)			
Voigt	149.89	137.05	123.87	114.58	90.86	112.17	70.32
Reuss	134.79	121.46	105.66	102.65	78.20	76.05	40.30
Hill	142.34	129.26	114.76	108.61	84.53	94.11	55.31

[a] P. S. Ntoahae [78]
[b] This work (equation of state from CASTEP calculation)

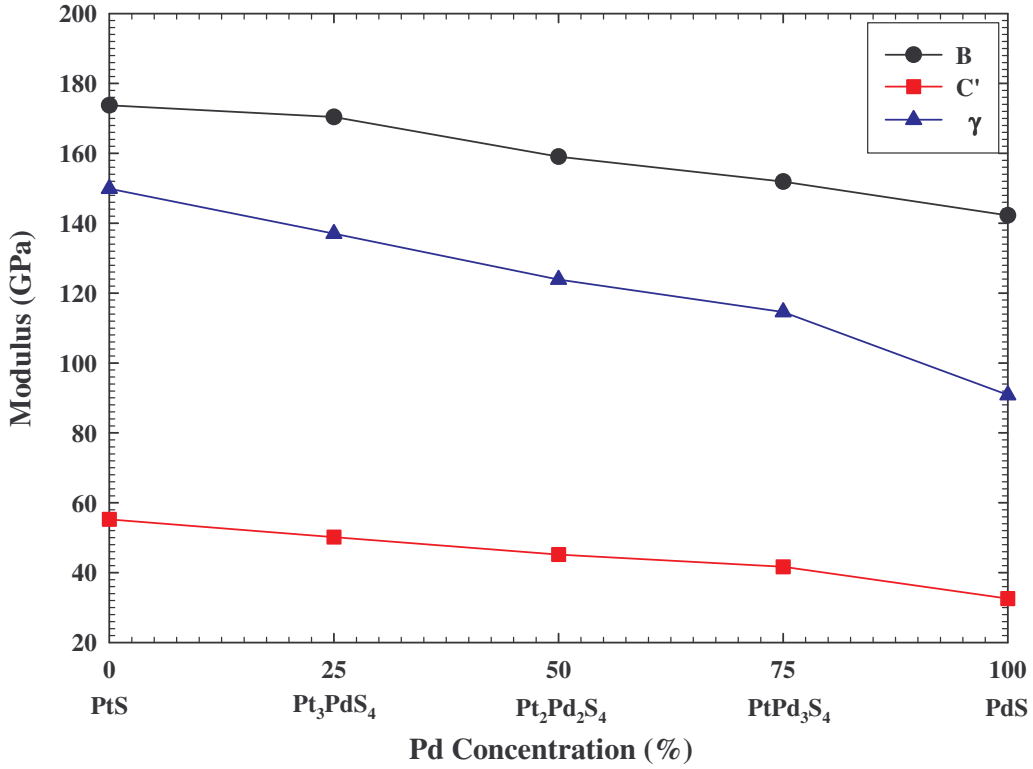

Figure 4.4 Variation of Pd concentration on bulk, shear and Young's modulus.

4.3.2 Heats of Formation

The heat of formation is the heat released or absorbed (enthalpy change) during the formation of a pure substance from its elements. It is one of the prime thermodynamic ingredient in the free energy to determine phase diagrams, the other being entropy. Hence studying the relative stability of binary and ternary compounds, it is convenient to consider the formation energy (E_{form}) of each structure. The formation energy is responsible for the relative stability of the phases at low temperatures where entropic contributions are not

important. These relative stabilities of different phases are determined through the well-known common tangent rule [82]. The heat of formation may be calculated by subtracting the total energies of the elemental systems from that of the compound. That is, the heat of formation per atom of a compound $(M,N)_8 S_8$ is given by

$$\begin{aligned}\Delta H_f((M,N)_8 S_8 &\equiv \Delta H_f(M_x N_{8-x} S_8 \\ &= \frac{1}{16}\left[E(M_x N_{8-x} S8) - xE(M) - (8-x)E(N) - 8E(S)\right]\end{aligned} \tag{4.1}$$

where M,N are chosen from Pd or Pt elements and, x and $(8-x)$ refer to the concentrations of constituent elements. Heats of formation have been computed to probe the presence of miscibility gap. Experimental heats of formation have been reported for PdS only by Zubkov et al. [3]. The current ab initio calculated heats of formation is -78.93 kJ/mol and compares very well with the experimental value of -78.1 kJ/mol. The calculated heats of formation of other binary and ternary compounds are displayed in table 4.4. Although PtS (cooperite) is an experimentally known structure, our calculations predict that PtS with vysotskite (PdS) structure is more stable.

Table 4.4 Heats of formation for binary and ternary compounds from PtS to PdS.

Compounds	Concentration %Pd	Space group	Calc. ΔH_f kJ/mol	Exp. [3] ΔH_f kJ/mol
PtS	0	P42/m	-82.92	-
$PdPt_3S_4$	25	P42/m	-332.31	-
$Pd_2Pt_2S_4$	50	P42/m	-163.84	-
Pd_3PtS_4	75	P42/m	-323.26	-
PdS	100	P42/m	-78.93	-78.1
PtS	0	P42/mmc	-82.42	-
PdS	100	P42/mmc	-71.41	-

Figure 4.5 shows the variation of heats of formation with Pd concentrations. No miscibility gap is noted between PtS (cooperite) and PdS (vysotskite) however, a continuum solid composition exists, which is in agreement with the experimental results by Merkle and Verryn [81]. We further observe that PtS (P42/m) has a lower energy as compared to PtS (P42/mmc), which suggests that PtS may also adopt a PdS structure. Additional experiments are needed to confirm our prediction.

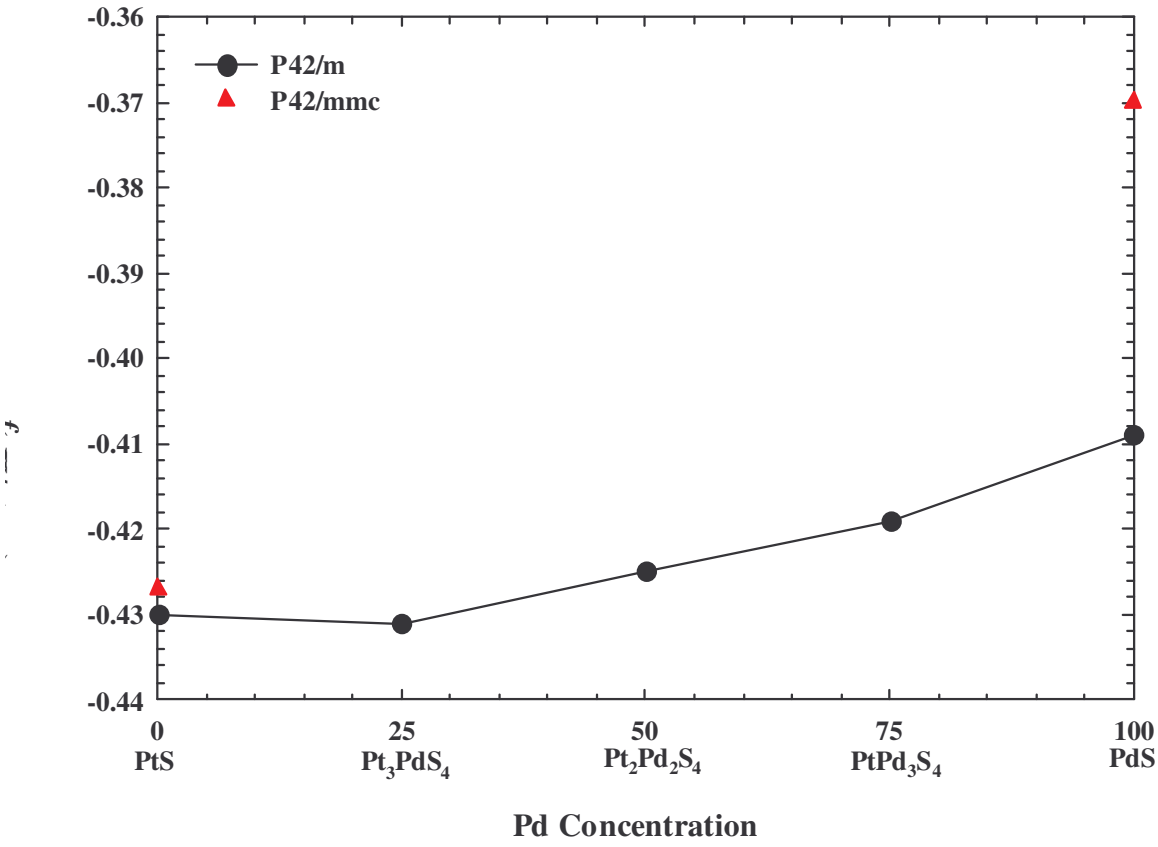

Figure 4.5 Heats of formation (ΔH_f) $Pd_{4-x}Pt_xS_4$ as a function of Pd concentration

4.3.3 Pseudogap at the Fermi Energy

Raybaud et al. [9] reported that the formation of a deep pseudogap at the Fermi level is the driving electronic mechanism for stabilization of the PdS and PtS monosulphides. Hence it is important for us to study the electronic properties of these binary and ternary compounds from PdS to PtS and check if there is a formation of deep pseudogap at the Fermi level. The total densities of states for binary and ternary compounds are plotted in figure 4.6 and the Fermi energy has been taken as the energy zero. This pseudogap can be clearly observed with respect to the Fermi energy. It is noted that the Fermi level falls at a deep pseudogap for PtS (P42/m), $PdPt_3S_4$ (P42/m), Pd_3PtS_4 (P42/m), PdS (P42/m), PtS (P42/mmc) and PdS (P42/mmc). However, the Fermi level for $Pd_2Pt_2S_4$ (P42/m) is slightly shifted owing to the pseudogap moving to lower energy. We extend our discussion by comparing the total and partial density of states of PdS (P42/m) with PdS (P42/mmc) and PtS (P42/m) with PtS (P42/mmc), which appear in figure 4.7. It is clear from the total density of states that they all have a deep pseudogap at the Fermi level. Looking at the partial density of states for PdS (P42/m and P42/mmc), peaks ranging from -15 eV to -12 eV corresponds mainly to S (3s) states. The broader distribution between -7 eV and valance band maximum (VBM) emanate predominantly from the S (3p) and Pd (4d) states. In the conduction band, the peaks from 0.25 eV to 1.55 eV for PdS (P42/mmc) and peaks from 0.25 eV to 3.2 eV corresponds to S (3p) and Pd (4d). For PtS (P42/m and P42/mmc), peaks ranging from -15.5 eV to -14.25 eV correspond to the S (3s). The broader distribution between -9 eV and VBM emanate predominantly from the S (3p) and Pt (5d) states.

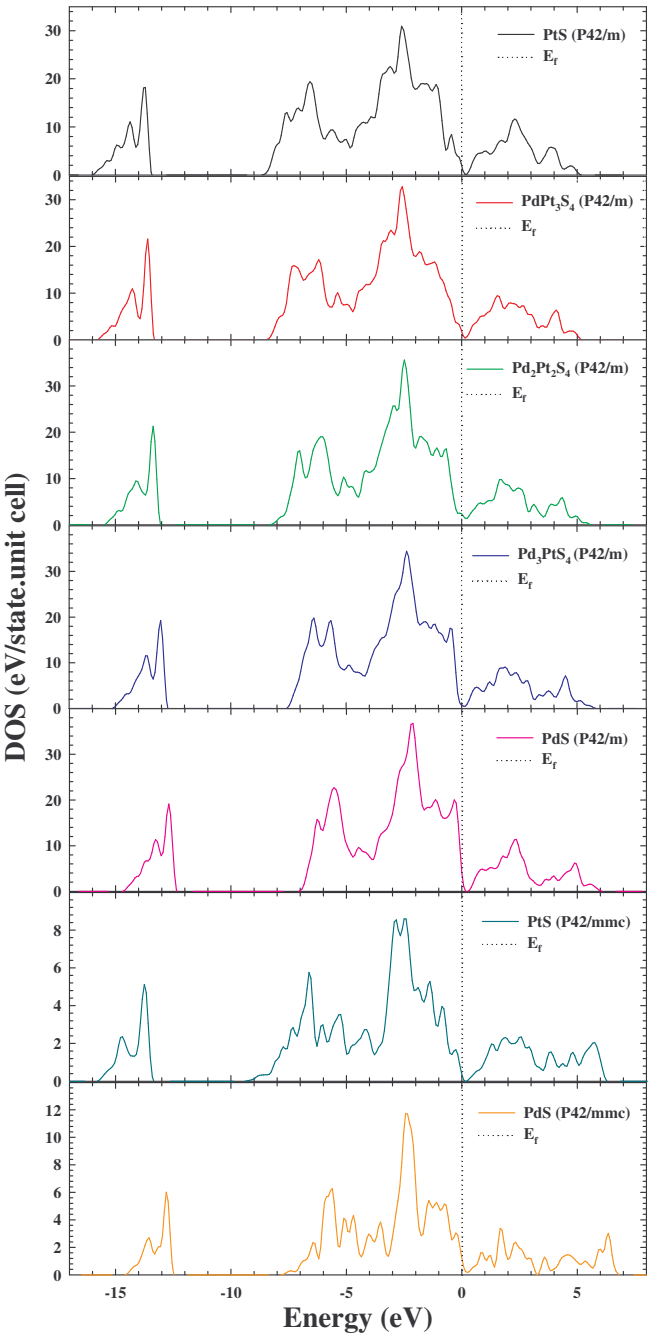

Figure 4.6 Total density of states for binary and ternary compounds from PtS to PdS.

In the conduction band, peaks from 0.5 eV to 5 eV for PtS (P42/m) and peaks from 0.5 eV to 6 eV for PtS (P42/mmc) corresponds to S (3p) and Pt (5d). The electronic partial densities of states of sulphur S (3p) orbital for the structure with space group P42/m has a soft hump but for the structure with space group P42/mmc there is sharp hump. This could be due to the structure differences.

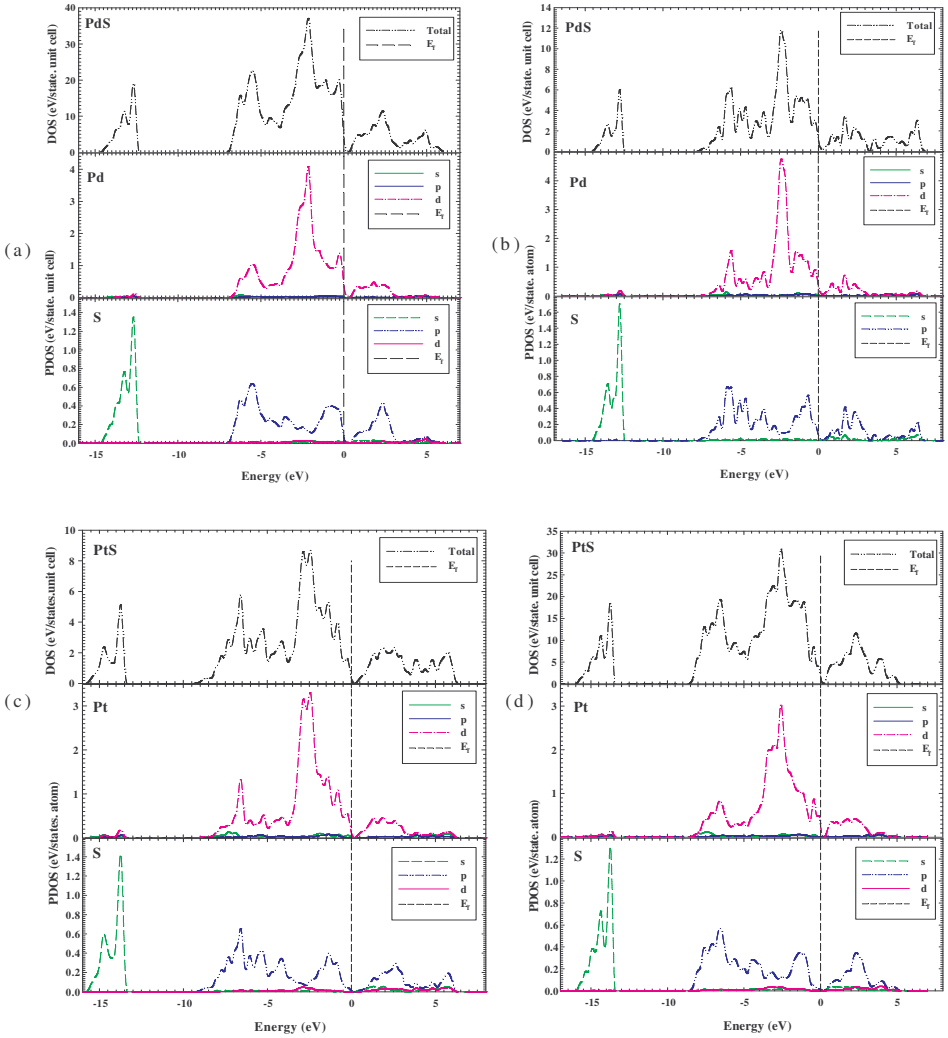

Figure 4.7 Total and partial density of states for PdS. (a) PdS (P42/m), (b) PdS (P42/mmc), (c) PtS (P42/mmc) and (d) PtS (P42/m).

Chapter 5

Conclusion and Recommendations

5.1 Conclusion

Density functional methods have been successfully used to investigate structural, electronic and optical properties of binary and ternary compounds from PtS to PdS. Our results are in good agreement with the available experimental results. Structural properties are comparable with the experimental values, since the predicted values are within 97% of accuracy. When pressure increases the lattice parameters decreases. We note a good correlation between calculated electronic and optical properties. Both of them predicts energy gap of 0.6 eV which is within the experimentally measured value of 0.02 eV and 2 eV [4, 5, 7, 9]. The band gap remained constant under variation of pressure, whilst the peaks just below and above the Fermi energy move. From the charge density differences of PdS, we noted covalent bonding between palladium and sulphur, and most charge transfer is from palladium to sulphur. Interpretation of the calculated reflectivity spectra is assisted by comparison with the experimental data which are in agreement and a deviation of approximately 5.5 % is noted at lower wavelengths, but at higher wavelengths the deviation is about 2.5 %. The compositional variation shows that both platinum and nickel, when located at 2a position in PdS unit cell, reduces the reflectance towards the experimental

value with nickel giving a better correlation. We have investigated the miscibility gap between binary and ternary compounds from PtS to PdS. Our results show no obvious gap but a continuum solid solution between these compounds, which is in agreement with the results compiled by Merkle and Verryn [81]. We have studied stability of the compound by computing heats of formations, elastic properties and densities of states. Most importantly, our first principle heat of formation of PdS (-78.93 kJ/mol) is in agreement with the experimental results of PdS (-78.1 kJ/mol) by Zubkov et al. [3]. Elastic constants for binary and ternary compounds, from PtS to PdS, meet the stability requirement for a tetragonal crystal under any homogeneous elastic deformation [69]. Our calculated bulk modulus (VASP) for PdS compare well with that obtained from the equation of state (CASTEP), unfortunately no experimental results are available for comparison. We observe that our calculated moduli (bulk, shear and Young's) decrease with increasing pressure. The density of states reflects a deep pseudo gap at the Fermi level, which is a driving force for stability of these monosulphides compounds [9] except for $Pd_2Pt_2S_4$ which is less stable.

5.2 Recommendations.

Structural, electronic and optical properties of PGMs have been studied extensively using ab initio methods. However, we would like to put forward some recommendations emanating from the current study. We have calculated bulk moduli and elastic constants which are of great interest, since such properties will contribute significantly in the development of inter-atomic potentials, which could initiate studies of pressure and

temperature dependence of thermodynamic properties of these compounds. We hope that our calculations will stimulate more experimental work on elastic constants and bulk moduli. The availability of such results will enable a meaningful validation of our predictions.

Bibliography

[1] A. J. Criddle, and C. J. Stanley, Can. Mineral. **23**, 149 (1985).

[2] L. J. Cabri, Miner. Sci. Eng. **4**(3), 3 (1972).

[3] A. Zubkov, T. Fujino, N. Sato, and K. Yamanda, J. Chem. Thermodyn. **30**, 571 (1998).

[4] I. J. Ferrer, P. Díaz-Chao, A. Pascual, and C. Sánchez, Thin Solid Films (2007), doi:10.1016/j.tsf.2006.12.079.

[5] J. C. W. Folmer, J. A. Turner, and B. A. Parkison, J. Solid State Chem. **68**, 28 (1987).

[6] R. Yamamoto 1986 : R. Yamamoto, Japanese Patent S61-215661 (1986).

[7] S. Dey and V. K. Jain, Platinum Metals Rev. **48**(1), 16 (2004).

[8] D. Nguyen-manh, P. S. Ntoahae, D. G. Pettifor, and P. E. Ngoepe, Mol. Simul. **22**, 23 (1999).

[9] P. Raybaud, J. Hafner, G. Kresse, and H. Toulhoat, J. Phys.: Condens. Matter. **9**, 11107 (1997).

[10] N. E. Brese, P. J. Squattrito, and J. A. Ibers, Acta Crystallogr. **C41**, 1829 (1985).

[11] P. Raybaud, G. Kresse, J. Hafner, and H. Toulhoat, J. Phys.: Condens. Matter. **9**, 11085 (1997).

[12] A. D. Genkin, and O. E. Zvyagintsev, Zapiski Vses. Mineralog. Obshch. **91**, 718

(1962).

[13] T. F Gaskell, Z. Kristallogr. **96**, 203 (1937).

[14] L. J. Cabri, J. H. G. Laflamme, J. M. Stewart, K. Turner, and B. J. Skinner, Am. Mineral. **63**, 832 (1978).

[15] J. D. Childs, and S. R. Hall, Acta Crystallogr. **B29**, 1446 (1973).

[16] H. Kyama and T. Iwata, Mitsubishi Paper Mills Ltd, Japanese Patent 08/095, 209 (1996).

[17] O. Tanabe, Fuji Photo Film Co Ltd, U.S. Patent 5, 030, 545 (1991).

[18] A. D. Genkin, Minerals of the Platinum Metals and their Associations in the Copper-Nickel Ores of the Noril'sk Deposits. Nauka, Moscow (in Russ.) (1968).

[19] L. N. Vyalsov, Acad. Sci. USSR, Inst. Geol. Petrog. Mineral. Geochem. Ore Deposits, Moscow (in Russ.) (1973).

[20] E. Wimmer : E. Wimmer, NATO Series: Electronic Structure Methods (1996).

[21] A. J. Freeman (1995) : A. J. Freeman, and E. Wimmer, Annu. Rev. Mater. Sci., **25**, 7 (1995).

[22] L. J. Thomas, Proc. Cam. Phil. Soc., **23**, 542 (1926).

[23] Fermi (1928) : I. J. Fermi, Z. Phys., **48**, 73 (1928).

[24] P. Hohenberg, and W. Kohn, Phys. Rev., **136**, 864B (1964).

[25] W. Kohn, and L. J. Sham, Phys. Rev., **140**, 1133A (1965).

[26] J. C. Slater, Phys. Rev., **81**, 385 (1951).

[27] J. C. Slater, Quantum Theory of Molecules and Solids Vol. **4**, McGraw-Hill, New York (1974).

[28] D. R. Hartree, Proc. Camb. Phil. Soc., **24**, 89 (1928).

[29] V. Fock, Z. Phys. **61**, 126 (1930) and ibid., **62**, 795 (1930).

[30] A. E. Mattson, P. A. Schultz, M. P. Desjarlais, T. R. Mattsson, and K. Leung, Modell. Simul. Mater. Sci. Eng., **13**, R1 (2005).

[31] F. Bloch, Z. Physik, **57**, 545 (1929).

[32] A. D. Becke, Phys. Rev. **A 38**, 3098 (1988).

[33] J. P. Perdew, Phys. Rev. **B 33**, 8822 (1986).

[34] J. P. Perdew, and Y. Wang, Phys. Rev. **B 45**, 13244 (1992).

[35] J. P. Perdew, K. Burke, and M. Ernzerhof, Phys. Rev. Lett. **77**, 3865 (1996).

[36] J. Andzelm, and E. Wimmer, J. Chem. Phys. **96**, 1280 (1992).

[37] J. P. Perdew, and A. Zunger, Phys. Rev. **B 23**. 5048 (1981).

[38] D. M. Ceperly, and B. J. Alder, Phys. Rev. Lett., **45**, 566 (1980).

[39] E. Wimmer, Molecular Simulations Inc. documentation (1997).

[40] M. C. Payne, M. P. Teter, D. C. Allan, T. A. Arias, and J. D. Joannopoulos, Rev. Mod. Phys. **64**, 1045 (1992).

[41] M. L. Cohen, and V. Heine, Solid State Physics., **24**, 37 (1970).

[42] J. C. Phillips, Phys. Rev., **112**, 685 (1958).

[43] M. T. Yin, and M. L. Cohen, Phys. Rev. **B 25**, 7403 (1982).

[44] J. S. Lin, A. Qteish, M. C. Payne, and V. Heine. Phys. Rev. **B 47**, 1993.

[45] W. A. Harrison, Electronic Structure and the Properties of Solids, edited by Freeman, San Francisco (1980).

[46] J. D. Joannopoulos, T. H. Starkloff, and M. Kastner. Phys. Rev. Lett., **38**, 660

(1977).

[47] J. D. Joannopoulos, T. H. Starkloff, and M. Kastner. Phys. Rev. **B 16**, 52512 (1977).

[48] E. L. Shirley, D. C. Allan, R. M. Martins, and J. D. Joanopoulos. Phys. Rev. **B 40**, 3652 (1989).

[49] D. Vanderbilt, Phys. Rev. **B 41**, 7892 (1990).

[50] V. Milman, B. Winkler, J. A. White, C. J. Pickard, M. C. Payne, E. V. Akhmatskaya, and R. H. Nobes, Int. J. Quant. Chem., **77**, 895 (2000).

[51] Accelrys Inc., CASTEP users Guide, San Diego: Accelrys Inc., 2001.

[52] D. J. Chadi, and M. L. Cohen, Phys. Rev. **B 8**, 5757 (1973).

[53] J. D. Joannopoulos, and M. L. Cohen, J. Phys. **C 6**, 1572 (1973).

[54] R. A. Evarestov, and V. P. Smirnov, Phys. Status. Solidi., **119**, 9 (1983).

[55] H. J. Monkhorst, and J. D. Pack, Phys. Rev. **13**, 5188 (1976).

[56] P. E. Blöchl, Phys. Rev. **B 50**, 17953 (1994).

[57] N. D. Mermin, Phys. Rev. **137**, A1441 (1965).

[58] P. Pulay, Chem. Phys. Lett., **73**, 393 (1980).

[59] C. G. Broyden, Math. Comput., **19**, 577 (1965).

[60] R. Car, and M. Parrinello, Phys. Rev. Lett. **55**, 2471 (1985).

[61] G. Kresse, and J. Furthmüller, Phys. Rev. **B 54**, 11169 (1996).

[62] G. Kresse, and J. Furthmüller, Computat. Mat. Sci., **6**, 15 (1996).

[63] G. Kresse, and D. Joubert, Phys. Rev. **B 59**, 1758 (1999).

[64] P. Ravindran, L. Fast, P. A. Korzhavyi, B. Johansson, J. Willis, and O. Eriksson, J.

Appl. Phys., **84**, 4891 (1998).

[65] M. J. Mehl, B. M. Klein, and D. A. Papaconstantopoulos, Intermetallic Compounds: vol. **1**, Principles. Edited by J. H. Westbrook and R. L. Fleischer, 1994, John Wiley & Sons Ltd.

[66] N. W. Ashcroft and N. D. Mermin, Solid State Physics, Saunders College, Philadelphia (1976).

[67] M. J. Mehl, Phys. Rev. **B 61**, 1654 (2000).

[68] J. F. Nye, Physical Properties of Crystals, Clarendon, Oxford (1957).

[69] D. C. Wallace, Thermodynamics of Crystals (Wiley, New York, 1972), Chapter 1.

[70] D. Iotova, N. Kioussis and S. P. Lim, Phys. Rev. **B 54**, 14413 (1996).

[71] S. F. Pugh : S. F. Pugh, Philos. Mag., **45**, 823 (1954).

[72] G. Kresse and J. Hafner, J. Phys.: Condens. Matter, **6**, 8245 (1994).

[73] C. G. Broyden, J. Inst. Math. Appl., **6**, 76 (1970).

[74] R. Fletcher, Comput. J., **13**, 317 (1970).

[75] D. Goldfard, Math. Comp., **24**, 23 (1970).

[76] D. F. Shanno, Math. Comp., **24**, 647 (1970).

[77] F. D. Murnaghan, Proc. Natl. Acad. Sci., **30**, 244 (1944).

[79] P. S. Ntoahae : P. S. Ntoahae, Application of Computer Simulation Methods to the Study of Platinum Group Minerals. PhD Thesis, University of Limpopo, Turfloop, South Africa (2005).

[79] S. M. C. Verryn, and R. K. W. Merkle, Applied Mineralogy in Research, Economy, Technology, Ecology, and Culture, AA Balkema, Rotterdam, 451

(2000).

[80] S. M. C. Verryn, and R. K. W. Merkle, Can. Mineral. **40**, 571 (2002).

[81] R. K. W. Merkle, and S. M. C. Verryn, Miner Deposita. **38**, 381 (2003).

[82] A. Cottrell, An Introduction to Metallurgy, Second Edition, 1975.

[83] J. Chen, L. L. Boyer, H. Krakauer, and M. J. Mehl, Phys. Rev. **B 37**, 3295 (1988).

[84] M. J. Mehl, and L. L. Boyer, Phys. Rev. **B 43**, 9498 (1991).

[85] O. H. Nielsen, and R. M. Martin, Phys. Rev. **B 32**, 3780 (1985); **32**, 3792 (1985).

[86] D. J. Vaughan, and J. R. Craig, Cambridge University Press, Cambridge, London-New York-Melbourne (1978).

Appendix A
Publications

N. O Monama and P. E. Ngoepe., Pressure dependence studies of structural, electronic and optical properties of PdS., to be submitted.

N. O. Monama and P. E. Ngoepe., Stability and mechanical properties of binary and ternary compounds from PtS to PdS., to be submitted.

Appendix B

Paper presented at conferences

N. O. Monama et al.," First principle study of structural and electronic properties of $AuSb_2$"., Presented at South African Institute of Physics (SAIP) 49th Annual Conference, held at the University of the Free State, in July 2004.

N. O. Monama et al., "Computational studies of Palladium sulphide"., Presented at Materials Modelling Meeting (MMM) 9th Annual Meeting, held at University of the North (S.A), in March 2005.

N. O. Monama et al., "Computational study of structural and electronic properties of Palladium sulphide"., Presented at South African Institute of Physics (SAIP) 50th Annual Conference, held at the University of Pretoria, in July 2005.

N. O. Monama et al., "Pressure dependence of structural and electronic properties of Palladium sulphide (PdS)"., Presented at Materials Modelling Meeting (MMM) 10th Annual Meeting, held at University of the North (S.A), in April 2006.

N. O. Monama et al., "Elastic, electronic, structural and optical properties of PdS"., Presented at South African Institute of Physics (SAIP) 51st Annual Conference, held at the University of Western Cape, in July 2006.

N. O. Monama et al., "Stability of PdS based structures"., Presented at South African Institute of Physics (SAIP) 52nd Annual Conference, held at the University of Witwatersrand, in July 2006.